arXiv:1109.5443v1 [physics.chem-ph] 26 Sep 2011

Auger decay of molecular double core-hole state

Motomichi Tashiro,[1, a)] Kiyoshi Ueda,[2] and Masahiro Ehara[3]

[1)] *Institute for Molecular Science, Nishigo-Naka 38, Myodaiji, Okazaki 444-8585, Japan*

[2)] *Institute of Multidisciplinary Research for Advanced Materials, Tohoku University, Sendai 980-8577, Japan*

[3)] *Institute for Molecular Science, Nishigo-Naka 38, Myodaiji, Okazaki 444-8585, Japan*

(Dated: 27 September 2011)

We report on theoretical Auger electron kinetic energy distribution originated from sequential two-step Auger decays of molecular double core-hole (DCH) state, using CH_4, NH_3 and H_2CO molecules as representative examples. For CH_4 and NH_3 molecules, the DCH state has an empty 1s inner-shell orbital and its Auger spectrum has two well separated components. One is originated from the 1st Auger transition from the DCH state to the triply ionized states with one core hole and two valence holes (CVV states) and the other is originated from the 2nd Auger transition from the CVV states to quadruply valence ionized (VVVV) states. Our result on the NH_3 Auger spectrum is consistent with the experimental spectrum of the DCH Auger decay observed recently [Phys. Rev. Lett. **105**, 213005 (2010)]. In contrast to CH_4 and NH_3 molecules, H_2CO has four different DCH states with $C1s^{-2}$, $O1s^{-2}$ and $C1s^{-1}O1s^{-1}$ (singlet and triplet) configurations, and its Auger spectrum has more complicated structure compared to the Auger spectra of CH_4 and NH_3 molecules. In the H_2CO Auger spectra, the $C1s^{-1}O1s^{-1}$ DCH $\rightarrow$ CVV Auger spectrum and the CVV $\rightarrow$ VVVV Auger spectrum overlap each other, which suggests that isolation of these Auger components may be difficult in experiment. The $C1s^{-2}$ and $O1s^{-2}$ DCH $\rightarrow$ CVV Auger components are separated from the other components in the H_2CO Auger spectra, and can be observed in experiment. Two-dimensional Auger spectrum, representing a probability of finding two Auger electrons at specific pair of energies, may be obtained by four-electron coincidence detection technique in experiment. Our calculation shows that this two-dimensional spectrum is useful in understanding contributions of CVV and VVVV states to the Auger decay of molecular DCH states.

[a)] Author to whom correspondence should be addressed. Electronic mail:tashiro@ims.ac.jp

I. INTRODUCTION

Molecular double core-hole (DCH) state is a state of a molecule with two inner-shell vacancies; they mostly correspond to two K-shell vacancies in the literature,[1–11] although two L-shell vacancies or one K-shell and one L-shell vacancies have been treated as well.[12] Two different kinds of molecular DCH state exist: single-site (ss) DCH state having core-hole vacancies at the same atomic site and two-site (ts) DCH state with two core-hole vacancies at different atomic sites. Properties of molecular DCH state with K-shell vacancies was first studied by Cederbaum et al.[1] at 1986 and have been discussed occasionally since then.[2–7] In contrast, experimental realization of probing molecular DCH state has not been possible until recently because of technological difficulties. Recently, X-ray free electron laser (XFEL) at Linac Coherent Light Source (LCLS) started operation,[13] which has capability to generate high intensity, short laser pulses required to produce molecular DCH state by sequential two-photon two-electron ionization. Using this XFEL facility, Fang et al.[8] identified the ss-DCH state of nitrogen molecule by analyzing photoelectron and Auger electron spectra. Cryan et al.[9] also obtained the Auger electron angular distribution originated from the N_2 DCH Auger decay in the molecular frame. At the same time, it has become possible to study molecular DCH state using synchrotron radiation (SR), combined with multi-electron coincidence technique. In contrast to two-photon sequential ionization by XFEL, SR mainly creates molecular ss-DCH state through single-photon two-electron ionization process. Eland et al.[10] detected the ss-DCH states of NH_3 and CH_4 molecules in their SR experiment. For NH_3 molecule, they obtained the Auger electron spectrum originated from the cascade Auger decay of the ss-DCH state. The 2h-1p pre-edge resonance state of NH_3, with double core-hole single electron valence excited configuration, was also identified, where they found that the state decays predominantly through the spectator Auger process. In different SR experiment, Lablanquie et al.[11] determined binding energies of the ss-DCH states for N_2, O_2, CO and CO_2 molecules. Using the four-electron coincidence detection method, with two photoelectrons and two Auger electrons, they obtained two-dimensional (2D) Auger intensity distribution of the N_2 ss-DCH decay as functions of two Auger electron kinetic energies. Their photoelectron spectrum of N_2 shows clear signature of the DCH shake-up satellite states. Based on the Auger spectrum of the N_2 DCH satellite state, they concluded that the satellite state decays by the spectator Auger process. Although number

of experimental studies on molecular DCH state is still limited, it is expected to increase in near future because XFEL facilities are being constructed in Japan and EU,[14] and also because more SR experiment will be performed to study molecular DCH state.

Several theoretical studies[1–7,15] have been performed on molecular DCH state to clarify its basic properties. As in single core-hole state, molecular DCH state is not stable but decays by Auger electron emission or X-ray emission, where Auger decay is expected to be dominant for low-Z elements.[16] At present, number of theoretical works on Auger decay of molecular DCH state is quite limited, where only two studies exist: theoretical N_2 DCH Auger spectrum by Fang et al.[8] and characterization of transient and final ion states in CH_4 and NH_3 DCH Auger decays by Eland et al.[10] Detailed knowledge about Auger electron kinetic energy distribution, such as assignment of peaks and prediction of Auger intensity, is important to interpret experimental molecular DCH Auger spectrum, in which single core-hole Auger spectrum or other instrumental noise often prevents straitforward extraction of DCH Auger spectrum.[10] In addition, detailed theoretical information may be valuable for studying time-dependent process of molecular DCH formation and decay in XFEL experiment.

Auger decay of molecular DCH state mainly involves three different kinds of electronic states:[10,11] DCH state, triply ionized states with one core hole and two valence holes (CVV states) and quadruply valence ionized (VVVV) states. These electronic states and their relations are schematically shown in Fig. 1. In the first Auger transition, the DCH state decays to the CVV states, then these CVV states decay to the VVVV states in the second Auger transition. Thus, two Auger electrons are emitted in molecular DCH Auger decay, in contrast to one Auger electron emission in Auger decay of single core-hole state. Other processes may also be involved in molecular DCH decay, such as X-ray emission, double Auger process[17] where a valence electron fills the vacant core-hole with emission of two Auger electrons, or direct Auger decay from DCH state to VVVV state where two valence electrons simultaneously fill the vacant core-holes with an emission of an Auger electron. These processes are not treated in the present work, because the probability of X-ray emission is expected to be small for low-Z elements treated in the present work. Aso, description of the double Auger process and the direct Auger decay from DCH state to VVVV state requires the second order perturbation in terms of the Coulomb interaction,[18] and thus their transition probabilities are expected to be small compared to normal Auger process which can be described by the first order perturbation.

In this work, Auger electron kinetic energy distributions are calculated and analyzed for the DCH states with K-shell vacancies of CH_4, NH_3 and H_2CO molecules. Auger decay in CH_4 and NH_3 involves only ss-DCH state. Auger decay in H_2CO, on the other hand, involves both ss- and ts-DCH states and therefore more complex Auger spectrum is expected. Although number of molecules is limited, our results may provide useful insights to discuss Auger decays of DCH states in other molecules.

We employ the complete active space self-consistent field (CASSCF) and configuration interaction (CASCI) methods to evaluate energies of DCH, CVV and VVVV states. The experimental ionization energies of the ss-DCH states have been measured for several molecules[10,11] and have been well reproduced by the CASSCF method.[5,10] Also, the CVV and VVVV energies of NH_3 obtained by the CASSCF and CASCI calculations roughly coincide with the peak positions in the experimental DCH Auger spectrum.[10] In order to obtain theoretical Auger electron kinetic energy distribution, we have to calculate Auger intensiies other than the energies of the DCH, CVV and VVVV states. In the present work, we directly evaluate Auger amplitude in the Wentzel's formula, where the initial and the final states are represented by multi-configuratinal wave functions. As we will show in section II, the Auger amplitude is represented by a linear combination of two-electron integrals with core-hole, valence and continuum Auger electron orbitals. In the literature of molecular single core-hole (SCH) Auger decay, explicit evaluation of continuum Auger orbital has been limited to a few theoretical works,[19–22] since treatment of such orbital in molecular system is rather difficult. Instead, several approximate methods have been introduced to avoid this difficulty. For instance, the molecular orbital of Auger electron is replaced by an continuum Auger orbital in atomic system.[23,24] The Stieljes imaging method was also employed[25] to represent continuum orbital in L^2 basis set. In other case, atomic population of valence orbitals is utilized to estimate absolute or relative Auger transition intensities,[26–29] in which continuum orbital is not evaluated at all. In this work, the intensities of DCH $\rightarrow$ CVV and CVV $\rightarrow$ VVVV Auger decays are approximated by using atomic population of valence orbitals, which was originally introduced for molecular SCH Auger decay by Mitani et al.[29] Although this approximation is not so accurate, it will be suitable to survey characteristic feature of Auger electron spectrum originated from molecular DCH Auger decay.

II. THEORETICAL METHOD

A. Auger Intensity

Kinetic energies of Auger electrons can be evaluated using standard quantum chemistry method for bound electronic state. In the present work, we employ the CASSCF and CASCI methods to obtain Auger electron energies. Estimation of Auger transition intensity, on the other hand, is not so straitforward as in evaluation of Auger electron kinetic energy. As in other theoretical works in molecular core-hole decay,[21,22,28–30] intensities of DCH $\rightarrow$ CVV Auger decay and subsequent CVV $\rightarrow$ VVVV Auger decay are evaluated by the Wentzel's formula,[31]

$$I_{fi} = 2\pi \left| \langle \Psi_f | \hat{H} - E | \Psi_i \rangle \right|^2 \equiv 2\pi \left| t \right|^2 , \tag{1}$$

where Ψ_i and Ψ_f are the wave functions for the initial and the final state, $\hat{H}$ is the Hamiltonian, E is the energy of the initial state, and t is the amplitude of the Auger transition. Atomic units are used in this expression. The wave function for the initial core-hole state, Ψ_i, is represented by a single or multi configurational N electron function with bound molecular orbitals (MOs), where N is the number of electrons in the initial state. In contrast, the wave function for the final state is in general represented as $\Psi_f = A \sum_a \Phi_a \phi_a$, where Φ_a is $N-1$ electron wave function for the final ion state a, ϕ_a represents continuum function for Auger electron in channel a, and A is antisymmetlization operator. In this work, we employ single-channel expression of the final state Ψ_f in which we include only one final ion state Φ_a. When we calculate an intensity of Auger transition between the initial state Ψ_i and the final ion state Φ_a, the final state wave function is just represented as $\Psi_f = A\Phi_a\phi_a$ under the single-channel expression. Further discussion on this subject can be found in Ref. 30 and references therein. In the present work, we used DCH and CVV state for Ψ_i and Φ_a, respectively, in calculation of DCH $\rightarrow$ CVV Auger intensity. Similarly, we used CVV and VVVV state for Ψ_i and Φ_a, respectively, in calculation of CVV $\rightarrow$ VVVV Auger intensity.

Before going into detail of actual Auger intensity calculation, we show below that convenient short expressions are available for DCH $\rightarrow$ CVV Auger amplitude, when the initial DCH state and the final CVV ion state are represented by single configurational state functions (CSFs) and the frozen orbital approximation is adopted. Although these short expressions were not used to calculate Auger intensity in the present work, we used them

to interpret and analyze our Auger spectra. In case of SCH Auger decay, it is well known that the Auger amplitude t in Eq. (1) has convenient short expressions when the initial and the final ion states are represented by single CSFs.[23,29,30,32] Assuming that the doublet SCH state is prepared by inner-shell ionization of closed-shell molecule, the Auger amplitude for the singlet final ion state with two vacancies in the v and w valence MOs is,

$$t = \sqrt{\frac{1}{2}}\left[(kv|cw) + (kw|cv)\right] \quad (v \neq w)\,, \tag{2}$$

$$= (kv|cv) \quad (v = w)\,. \tag{3}$$

For triplet final ion state, the amplitude is

$$t = \sqrt{\frac{3}{2}}\left[(kv|cw) - (kw|cv)\right]. \tag{4}$$

Here c and k represent MOs for the core-hole vacancy and the continuum Auger electron, respectively. The expression $(ij|kl)$ represents two-electron integral,

$$(ij|kl) = \int dr_1 dr_2 \phi_i\left(r_1\right)\phi_j\left(r_1\right)\frac{1}{r_{12}}\phi_k\left(r_2\right)\phi_l\left(r_2\right), \tag{5}$$

which involves MOs ϕ_i, ϕ_j, ϕ_k and ϕ_l. In a similar manner, we can derive expression for amplitudes of Auger transition from DCH state to CVV state, assuming frozen orbital approximation as well as single CSF wave functions. The results are summarized in Table I. We selected a specific spin-coupling scheme to represent doublet CVV states in Table I, where intermediate spin state, singlet or triplet, was first formed in valence electrons, then it was coupled with doublet core electron to form total spin state with S=1/2. In other word, we represent two S=1/2 wave functions as $\Phi_S = 1/\sqrt{2}\left(|v\bar{w}c| - |\bar{v}wc|\right)$ and $\Phi_T = 1/\sqrt{6}\left(|v\bar{w}c| + |\bar{v}wc| - 2\,|vw\bar{c}|\right)$. Spin-coupling scheme is not unique when we construct total spin state from three S=1/2 particles.[33] For example, the wave functions Φ_S and Φ_T shown above are constructed from spin coupling scheme $vw \cdot c$, which means that v and w orbitals form singlet or triplet configuration, then c orbital couples this configuration. Similarly, other spin coupling scheme such as $v \cdot wc$ or $cv \cdot w$ is possible. So, care must be taken when expressions in Table I are compared with other calculation. The expressions in Table I are very similar to those of the SCH Auger amplitudes, i.e., addition of two-electron integrals appears in the expression when valence electrons are coupled to form singlet, while subtraction of the integrals appears when valence electrons form triplet. From this observation, the Auger transition from DCH state to the CVV state with singlet intermediate

valence spin state is expected to be more intense than the transition to the CVV state with triplet intermediate spin state, as in the case of SCH Auger decay. Although it may be possible to derive similar expressions for CVV $\rightarrow$ VVVV Auger decay, we did not attempt it because there are too many combinations in orbitals. In the present work, we directly evaluated Eq. (1) using CI wave functions of CVV and VVVV states, as will be described below. Although the equations in Table I were not used in our actual calculation, they may be usefull in other theoretical or experimental work when quick evaluation of DCH $\rightarrow$ CVV Auger intensity is required.

When the initial and the final ion states are represented by more general multi configurational functions, the Auger amplitude is represented as

$$t = \sum_{v,w} C_{v,w} \left(kv|cw\right), \tag{6}$$

where the summation of MOs v and w is taken over all active valence orbitals. The coefficients $C_{v,w}$ depend on CI coefficients of the wave functions, determinant-CSF conversion coefficients, and relative ordering of MOs in determinants of the initial and final states. As in the case of single CSF wave functions, frozen orbital approximation was assumed in Eq. (6). We employ this frozen orbital approximation because of its computational efficiency. If we used non-orthogonal orbital sets, considering relaxation effect, then evaluation of Auger amplitude would be much difficult because of long calculation time. Discussion on validity of the frozen orbital approximation for single core-hole Auger decay can be found in Ref. 30 and references therein. In order to obtain Auger spectrum, we directly evaluated the Auger amplitudes t in Eqs. (1) and (6) in combination with multi-configurational expressions (CI wave functions) of the initial and the final states. Eqs.(1) and (6) can be used for any type of Auger transition involving one core-hole decay, two-valence hole creation and an emission of one Auger electron, which includes DCH$\rightarrow$CVV and CVV$\rightarrow$VVVV Auger decays as well as SCH$\rightarrow$VV Auger decay. It is important to recognize that $C_{v,w}$ in Eq. (6) contains the product of the CI coefficients of the initial and final ion state wave functions, thus only the CSFs with large CI coefficients contribute to the Auger amplitude t.

The two-electron integral $(kv|cw)$ in Eqs. (3),(4) and (6) contains MO k for the continuum Auger electron. We used the method described in Mitani et al.[29] which approximates this two-electron integral $(kv|cw)$ by the population of MO w on the atom A where the core-hole orbital c is localized. Although this approximation is not so accurate, it can reproduce

qualitative feature of the experimental SCH Auger spectra of H_2O and NH_3,[29] and will be appropriate to understand qualitative nature of DCH Auger spectrum as well.

B. Detail of the calculation

The energies of DCH, CVV and VVVV states as well as Auger intensities were evaluated by fixed bond length calculations. Since the lifetime of DCH and CVV states are expected to be similar or shorter than the lifetime of SCH state, e.g., less than 10 fs for C, N or O elements,[16] the effect of the vibrational motion may be small. Experimental geometries of CH_4, NH_3 and H_2CO molecules[34–36] were used in this work. Calculation for H_2CO molecule was performed with C_{2v} point group symmetry. Although CH_4 and NH_3 molecules belong to T_d and C_{3v} point group symmetries, respectively, we used D_2 and C_s symmetries in the calculations. The energies and CI coefficients of the CVV and VVVV states were obtained by the CASCI calculations using the MOs prepared by the state-averaged (SA) CASSCF[37,38] calculations for the low-lying CVV and VVVV states. For CH_4, 60 CVV and 300 VVVV states were obtained by the CASCI calculations based on the CASSCF calculations for the low-lying 12 CVV and 10 VVVV states, respectively. For NH_3, 100 CVV states were calculated by the CASCI method based on the CASSCF calculation for the low-lying 15 CVV states, and 300 VVVV states were obtained by the CASCI method using the MOs taken from the CASSCF calculation for the low-lying 11 VVVV states. For H_2CO, 1500 C1s^{-1} CVV, 1500 O1s^{-1} CVV and 3000 VVVV states were obtained by the CASCI calculations based on the CASSCF calculations for the low-lying 20 C1s^{-1} CVV, 24 O1s^{-1} CVV and 30 VVVV states, respectively. Note that these numbers refer to total numbers of calculated CVV or VVVV states in the molecules, i.e., summation of calculated states over all irreducible representations. These electronic states obtained by the CASCI calculations were sufficient to cover whole energy range of the DCH $\rightarrow$ CVV as well as the CVV $\rightarrow$ VVVV Auger spectra of CH_4, NH_3 and H_2CO. The cc-pVTZ basis set[39] was employed for all these calculations. We used frozen Hartree-Fock orbitals to represent 1s core orbitals, while the other orbitals were fully relaxed and optimized in the CASSCF calculations. As in our previous works on molecular DCH states,[5,6] all valence electrons were distributed in the active orbital space composed of all available valence MOs, while occupation of core-hole orbital was explicitly restricted. The same set of active orbitals was used in both the CASSCF and CASCI

calculations. The total number of active orbitals is 8, 7 and 10 for CH_4, NH_3 and H_2CO, respectively. With these active orbitals, typical number of configurations in the CVV states is 670, 550 and 12500 for CH_4, NH_3 and H_2CO, respectively. For the VVVV states, the number of CSFs is 90, 100 and 3500 for CH_4, NH_3 and H_2CO, respectively. The energies of the DCH states for CH_4, NH_3 and H_2CO were also obtained by the CASSCF calculations, using the same basis set and active orbitals as in the calculations for the CVV and VVVV states. Our CASSCF double ionization energies (DIEs) are 650.2, 891.0, 658.0 and 1168.5 eV for the CH_4 $C1s^{-2}$, NH_3 $N1s^{-2}$, H_2CO $C1s^{-2}$, and H_2CO $O1s^{-2}$ ss-DCH states, respectively. The DIE of the H_2CO $C1s^{-1}O1s^{-1}$ ts-DCH state is 846.6 eV for the singlet, and 847.0 eV for the triplet state. These DIEs were used to obtain the Auger kinetic energies of the DCH $\rightarrow$ CVV Auger decays. For these CASSCF and CASCI calculations, molpro program package[40] was mostly used. In addition, congen and scatci modules in the UK R-matrix codes[41] were partly used to analyze the electronic states.

In evaluation of the Auger intensities, we used the Löwdin atomic population of the MOs which were taken from the CASSCF calculation for the CVV states. The population obtained by the MOs for the VVVV states gave similar Auger intensities. Although choice of population, Löwdin or Mulliken, affects Auger intensities as demonstrated by Mitani et al.,[29] qualitative feature of the result does not change much. In Auger intensity evaluation using Eqs. (1) and (6), wave function of DCH state was approximated by a single CSF, since weights of the other configurations were small. For CVV and VVVV states, five configurations with the largest CI coefficients were taken into account in the Auger intensity evaluation. We performed a test calculation on CH_4 DCH Auger spectra, taking into account 30 configurations with the largest CI coefficients. The results obtained with 30 and 5 configurations are almost the same, as shown in Fig. S1. This indicates that inclusion of five configurations is enough in Auger intensity evaluation. The intensities of the 1st Auger transitions were normalized as $\sum_i I\left(\mathrm{DCH}, \mathrm{CVV}_i\right) = 1$ or 3, where the summation is 1 for the singlet ss- and ts-DCH states and 3 for the triplet ts-DCH state, and $I\left(\mathrm{DCH}, \mathrm{CVV}_i\right)$ is the intensity for transition from the DCH state to the final state with the ith CVV ion state. The normalization for the 2nd Auger intensities is $\sum_j I\left(\mathrm{CVV}_i, \mathrm{VVVV}_j\right) = I\left(\mathrm{DCH}, \mathrm{CVV}_i\right)$, where $I\left(\mathrm{CVV}_i, \mathrm{VVVV}_j\right)$ is the intensity for the transition from the ith CVV state to the final state with the jth VVVV ion state. This expression for normalization of the 2nd Auger intensity indicates that two conditions should be satisfied at once in order to have large in-

tensity in the 2nd Auger decay; (1) The ith CVV state is populated enough in the 1st Auger decay, or, $I\,(\mathrm{DCH}, \mathrm{CVV}_i)$ is large enough, and (2) The ith CVV state and the jth VVVV ion state have enough transition moment in Eq. (1), or, $I\,(\mathrm{CVV}_i, \mathrm{VVVV}_j)$ is large enough. These two conditions severely restrict possible pair of CVV and VVVV states which has noticeably large intensity in the 2nd Auger decay.

III. RESULTS AND DISCUSSION

A. CH_4

In Fig. 2, calculated CH_4 Auger intensities are shown as a function of Auger electron kinetic energy, where the 1st Auger transitions from the C1s^{-2} DCH state to the C1s^{-1} CVV states and the 2nd Auger transitions from the C1s^{-1} CVV states to the VVVV states contribute the spectrum. Since the main configuration of the CH_4 DCH state is $(1s)^0(2a_1)^2(1t_2)^6$, the $2a_1$ and $1t_2$ valence orbitals mainly participate to the Auger transitions. Main part of the DCH $\rightarrow$ CVV Auger spectrum extends from 270 to 290 eV, and the CVV $\rightarrow$ VVVV Auger spectrum extends from 210 to 240 eV. These two different Auger spectra are well separated in energy each other. Number of discrete Auger transitions, indicated as vertical bars in Fig. 2, is 6 for the DCH $\rightarrow$ CVV Auger decay and 300 for the CVV $\rightarrow$ VVVV Auger decay. The convoluted DCH $\rightarrow$ CVV Auger spectrum in Fig. 2, obtained by convolution of the discrete Auger spectrum with Gaussian having 4.5 eV width, has 3 large distinct peaks, whereas the convoluted CVV $\rightarrow$ VVVV Auger spectrum has 4 peaks. The highest energy peak ($\sim$ 295 eV) in the convoluted DCH $\rightarrow$ CVV Auger spectrum corresponds to the $(t_2)^{-2}$ valence vacancy creation. The second highest ($\sim$ 280 eV) and the 3rd highest ($\sim$ 270 eV) energy peaks in the DCH $\rightarrow$ CVV spectrum are formed by the $(2a_1)^{-1}(t_2)^{-1}$ and $(2a_1)^{-2}$ valence hole creations, respectively. The highest ($\sim$ 235 eV) and the lowest ($\sim$ 210 eV) energy peaks in the CVV $\rightarrow$ VVVV Auger spectrum originate from the $(t_2)^{-2}$ and $(2a_1)^{-2}$ vacancy creations, as in the DCH $\rightarrow$ CVV Auger case. Two peaks in the middle of the CVV $\rightarrow$ VVVV Auger spectrum are formed by the $(2a_1)^{-1}(t_2)^{-1}$ vacancy creation, where the initial states of the higher energy peak ($\sim$ 225 eV) have the $(2a_1)^1$ configurations and those of the lower energy peak ($\sim$ 220 eV) have the $(2a_1)^2$ configurations.

The kinetic energies of the 1st and 2nd Auger electrons have correlation because these

two Auger decays are not independent as shown schematically in Fig. 1. The upper panel of Fig. 3 shows 2D Auger intensity distribution as functions of the 1st and 2nd Auger electron kinetic energies, obtained by smoothing theoretical discrete Auger spectrum. Integration of this 2D Auger spectrum along the vertical axis (the 2nd Auger electron energy) gives the convoluted DCH $\rightarrow$ CVV Auger spectrum in Fig. 2, and integration along the horizontal direction (the 1st Auger electron energy) gives the CVV $\rightarrow$ VVVV Auger spectrum. In the upper panel of Fig. 3, several distinct and round-shaped high-intensity regions are recognized. The highest intensity region around the 1st Auger energy of 295 eV and the 2nd Auger energy of 235 eV corresponds to the $(1t_2)^{-2}$ valence hole creation followed by another $(1t_2)^{-2}$ valence hole creation in the successive two Auger transitions. Next to this highest intensity peak, there are three peaks with the 2nd highest Auger intensities. The peak around the 1st Auger energy of 295 eV and the 2nd Auger energy of 220 eV corresponds to the $(1t_2)^{-2}$ vacancy creation in the 1st Auger decay, followed by the $(2a_1)^{-1}(1t_2)^{-1}$ vacancy creation in the 2nd Auger decay. The peak at the 1st Auger energy of 280 eV and the 2nd Auger energy of 235 eV corresponds to successive formation of the $(2a_1)^{-1}(1t_2)^{-1}$ and the $(1t_2)^{-2}$ valence vacancies. The peak around the 1st Auger energy of 280 eV with the 2nd Auger energy of 225 eV is formed by the $(2a_1)^{-1}(1t_2)^{-1}$ vacancy creation followed by another $(2a_1)^{-1}(1t_2)^{-1}$ vacancy creation. Note that Lablanquie et al. reported the experimental 2D Auger spectrum for the ss-DCH Auger decay of N_2 molecule,[11] by measuring kinetic energies of the two Auger electrons. So far, such experimental 2D Auger spectrum is not available for the other molecules.

Binding energies of DCH state (E_{DCH}), CVV state (E_{CVV}) and VVVV state (E_{VVVV}) are related to the 1st and 2nd Auger electron kinetic energies (E_{Auger1} and E_{Auger2}) as, $E_{\mathrm{DCH}} = E_{\mathrm{CVV}} + E_{\mathrm{Auger1}}$ and $E_{\mathrm{CVV}} = E_{\mathrm{VVVV}} + E_{\mathrm{Auger2}}$. Using these relations as well as experimental or theoretical value of E_{DCH}, the 2D Auger spectrum in the upper panel of Fig. 3 can be converted to the 2D Auger spectrum as functions of CVV and VVVV binding energies, as shown in the lower panel of Fig. 3. In this plot, contributions of CVV and VVVV states to the Auger intensity can be easily recognized: the highest intensity peak at bottom left corner of the plot is related to the lowest energy CVV and VVVV states. for example. By integrating this 2D Auger spectrum along the horizontal axis (CVV energy), integrated one-dimensional (1D) Auger intensity as a function of VVVV binding energy can be obtained as shown in the lower panel of Fig. 4. Similarly, integration along the vertical

axis (VVVV energy) gives integrated 1D Auger intensity as a function of CVV binding energy as shown in the upper panel of Fig. 4. Although we need integration to extract these 1D spectra from experimental data, theoretical 1D spectra can be obtained directly from our calculation, without explicit integration. The original discrete spectra are shown as vertical bars in Fig. 4. Three distinct peaks are seen in both panels, with the highest energy peak corresponds to the $(2a_1)^0(1t_2)^n$ configuration, the second highest peak corresponds to the $(2a_1)^1(1t_2)^{n-1}$ configuration and the lowest energy peak corresponds to the $(2a_1)^2(1t_2)^{n-2}$ configuration, where n is 6 for the CVV states in the upper panel and 4 for the VVVV states in the lower panel.

For reference, ionization energies of the calculated CVV states are summarized in Table II with their main configurations and intensities for the 1st Auger decay. The VVVV states are not provided because there are too many states. Because of spin conservation in Eq. (1), the singlet ss-DCH state of CH_4 decays only to the doublet CVV states. When the wave functions of the DCH and CVV states are approximated by a single CSF, expressions of the ss-DCH $\rightarrow$ CVV Auger intensities can be classified into three different types as described in Sec. II.A and Table I. According to this classification, Auger intensity tends to be larger for the CVV final ion state with singlet intermediate spin state in valence electrons than that with triplet intermediate spin state in valence electrons. The calculated Auger intensities in Table II roughly obey this trend.

B. NH_3

In Fig. 5, calculated Auger spectrum of NH_3 DCH decay is shown as a function of Auger electron kinetic energy, which include contributions from the 1st Auger transitions from the N1s^{-2} DCH state to the N1s^{-1} CVV states and the 2nd Auger transitions from the N1s^{-1} CVV states to the VVVV states. For comparison, experimental NH_3 DCH Auger spectrum of Eland et al.[10] and theoretical Auger spectrum of NH_3 SCH $\rightarrow$ VV (doubly valence ionized states) Auger decay are also shown in the figure. The SCH Auger spectrum was calculated by the same procedure as we used for the DCH $\rightarrow$ CVV and CVV $\rightarrow$ VVVV Auger decays.

Main part of the theoretical DCH $\rightarrow$ CVV Auger spectrum extends from 380 to 420 eV, whereas the CVV $\rightarrow$ VVVV and SCH $\rightarrow$ VV Auger spectra extend from 300 to 350 eV and 335 to 375 eV, respectively. Although the CVV $\rightarrow$ VVVV and SCH $\rightarrow$ VV Auger spectra

overlap partly, the main part of the DCH → CVV Auger spectrum is well separated from the CVV → VVVV and SCH → VV spectra. Number of discrete Auger transitions, indicated as vertical bars in Fig. 5, is 14 for the DCH → CVV Auger decay, 23 for the SCH → VV Auger decay, and 995 for the CVV → VVVV Auger decay. Because of difference in number of transitions, discrete spectra of the DCH → CVV and CVV → VVVV Auger decays look rather different in Fig. 5. However, when these spectra are convoluted by Gaussian function, close similarity is observed between these two Auger spectra. Also, overall shape of the convoluted SCH → VV Auger spectrum resembles those of the convoluted DCH → CVV and CVV → VVVV Auger spectra. Compared to the position of the convoluted SCH → VV Auger spectrum, the DCH → CVV Auger spectrum is located about 50 eV higher in energy, and the CVV → VVVV spectrum is located about 20 eV lower in energy. Origin of the energy shift of the DCH → CVV Auger spectrum relative to the SCH → VV spectrum is mainly attributed to the Coulomb repulsion of the core holes, which increases the energy of the DCH state.[1,5] In addition, the CVV states are stabilized by existence of two valence holes which weaken the Coulomb screening of the nuclear charges. This stabilization contributes to the shift of the DCH → CVV Auger spectrum into the higher energy. The shift of the CVV → VVVV Auger spectrum to the lower energy can also be explained by this stabilization of the CVV states. Each convoluted Auger spectrum has 5 distinct peaks, which can be assigned in terms of the occupied valence MOs in the main configurations of the DCH and SCH states: the $2a_1$, $1e$ and $3a_1$ orbitals. The highest energy peak has the largest intensity, accompanying a faint shoulder structure at higher energy side. This shoulder structure corresponds to the Auger transition with $(3a_1)^{-2}$ valence vacancy creation, whereas the main peak corresponds to the $(1e)^{-1}(3a_1)^{-1}$ vacancy creation. The second highest energy peak, with the second largest intensity, originates from the $(1e)^{-2}$ vacancy creation. The 3rd, 4th and 5th peaks are formed by the $(2a_1)^{-1}(3a_1)^{-1}$, $(2a_1)^{-1}(1e)^{-1}$ and $(2a_1)^{-2}$ valence hole creations, respectively. The intensity of the 5th peak is much smaller than the other peaks.

The experimental spectrum of Eland et al.,[10] obtained by the triple electron coincidence method with synchrotron radiation, is compared with our results in Fig. 5. Although the experimental spectrum was plotted as a function of CVV binding energy in Ref. 10, we converted the spectrum as a function of Auger electron kinetic energy using the experimental NH_3 DCH binding energy of 892 eV. The large peak around 425 eV in the experimental

spectrum coincides well with the $(3a_1)^{-2}$, $(1e)^{-1}(3a_1)^{-1}$ and $(1e)^{-2}$ peaks in the calculated DCH $\rightarrow$ CVV Auger spectrum. The rise of experimental intensities around 400 eV may have relation with the $(2a_1)^{-1}(3a_1)^{-1}$ and $(2a_1)^{-1}(1e)^{-1}$ peaks in the calculated spectrum. The experimental intensity appears to increase at around 380 eV, where the calculated $(2a_1)^{-2}$ peak exists. However, association of this 380 eV peak with the calculated peak is not clear because of difference in intensities as well as experimental uncertainty. The experimental peaks around 360 - 370 eV coincide well with the calculated SCH $\rightarrow$ VV peaks with the $(3a_1)^{-2}$, $(1e)^{-1}(3a_1)^{-1}$ and $(1e)^{-2}$ vacancy creations. As noted by Eland et al.,[10] the origin of these peaks around 360 - 370 eV is secondary electrons created by the SCH $\rightarrow$ VV Auger electrons or photoelectrons of the SCH formation. Thus, the height of these peaks do not directly reflect the SCH formation cross section, which is much larger than the DCH formation cross section.[11] Also, the shape of the SCH related peaks may be distorted from the original SCH Auger spectrum, because of the process involved in the secondary electron creation. We just adjusted the height of the calculated SCH Auger spectrum to the experimental peak around 370 eV. There is a peak around 340 eV in the experimental spectrum, whose location is very close to the calculated CVV $\rightarrow$ VVVV Auger peaks with the $(3a_1)^{-2}$, $(1e)^{-1}(3a_1)^{-1}$ and $(1e)^{-2}$ vacancy creations. Although intensities are smaller, the $(2a_1)^{-1}(3a_1)^{-1}$ and $(2a_1)^{-1}(1e)^{-1}$ peaks in the SCH $\rightarrow$ VV Auger spectrum may also have contribution to the experimental peak at 340 eV. Below 330 eV, association of the calculated CVV $\rightarrow$ VVVV Auger spectrum and the experimental spectrum is not clear. Although agreement with the experimental spectrum and our result looks modestly good on the whole, some degree of discrepancy exists, especially around the 2nd Auger component. Origin of the difference may be related to the approximations employed in our calculation, e.g., the frozen orbital approximation or neglect of the shake-up satellite DCH states. By considering orbital relaxation or the satellite states, the shape of the theoretical Auger spectrum may be changed. In addition, experimental noise from SCH signal can be another source of the discrepancy, which may be reduced by performing four-electron coincidence experiment.

In the upper panel of Fig. 6, 2D Auger spectrum is shown as functions of the 1st and the 2nd Auger kinetic energies. Compared to the 2D Auger intensity distribution for the CH_4 DCH decay in Fig. 3, high-intensity regions look less distinct in the NH_3 Auger spectrum. For both the 1st and 2nd Auger electrons, the higher kinetic energy corresponds to vacancy

creation in the $3a_1$ and $1e$ orbitals, and the lower kinetic energy corresponds to vacancy creation in the $2a_1$ orbital. Thus, the highest-intensity region surrounded by the 1st Auger energies of 410 - 420 eV and the 2nd Auger energies of 340 - 350 eV mainly corresponds to the $(1e3a_1)^{-2}$ valence hole creation followed by another $(1e3a_1)^{-2}$ valence hole creation in the sequential two-step Auger decays. The second highest intensity regions are located next to the highest intensity region, one surrounded by the 1st Auger energies of 410 - 420 eV and the 2nd Auger energies of 320 - 335 eV, and the other surrounded by the 1st Auger energies of 390 - 405 eV and the 2nd Auger energies of 340 - 350 eV. The former corresponds to the $(1e3a_1)^{-2}$ valence hole creation followed by the $(2a_1)^{-1}(1e3a_1)^{-1}$ valence hole creation, and the later corresponds to the $(2a_1)^{-1}(1e3a_1)^{-1}$ valence hole creation followed by the $(1e3a_1)^{-2}$ valence hole creation.

As in the CH_4 case, the 2D Auger spectrum in the upper panel of Fig. 6 can be converted to the 2D intensity as functions of CVV and VVVV binding energies as shown in the lower panel of Fig. 6. This plot shows clearly that the highest intensity region corresponds to the low-lying CVV and VVVV states. Integration of the 2D Auger spectrum in the lower panel of Fig. 6 along the vertical or the horizontal axis gives the integrated 1D Auger spectra as shown in Fig. 7. The integrated Auger intensity as a function of CVV binding energy in the upper panel of Fig. 7 has 3 large peaks which correspond to the CVV states with $(2a_1)^2$, $(2a_1)^1$ and $(2a_1)^0$ configurations. The integrated Auger intensity as a function of VVVV binding energy in the lower panel has more complicated structure compared to the intensity in the upper panel. We can still make assignment of these peaks in terms of electronic configuration, e.g., the lowest energy peak corresponds to the configuration $(2a_1)^2(1e)^2(3a_1)^0$, the second lowest peak to the configuration $(2a_1)^2(1e)^1(3a_1)^1$, while the peaks in the middle of the spectrum are related to the $(2a_1)^1$ type configuration. Compared to the integrated 1D spectra of CH_4 VVVV states, the integrated 1D spectrum of NH_3 VVVV states is distributed broader and looks less structured. This difference is attributed to the different number of occupied valence orbitals in CH_4 (two orbitals) and NH_3 (three orbitals). This suggests that it may be hard for large molecule to recognize peak structure in integrated 1D spectra.

For reference, ionization energies of the calculated CVV states are listed in Table III with their main configurations and the intensities for the DCH $\rightarrow$ CVV Auger decay. As in the CH_4 case, the DCH $\rightarrow$ CVV Auger intensity tends to be larger for the CVV final ion states

with singlet intermediate valence spin than the ion states with triplet intermediate valence spin.

C. H_2CO

In Fig. 8, the Auger electron kinetic energy distribution of H_2CO is shown for the sequential Auger decays of the DCH and CVV states. In contrast to NH_3 and CH_4, H_2CO has four different DCH states: two ss-DCH states (singlet $C1s^{-2}$ and $O1s^{-2}$) and two ts-DCH states (singlet and triplet $C1s^{-1}O1s^{-1}$). We consider the case where these four DCH states are created in XFEL experiment. In order to simplify the situation, we just assumed that the formation probabilities are determined by statistical ratio: 1:3 for singlet and triplet DCH states. This approximation has been well known and discussed in the literate of inner-shell photoionization.[43,44] The formation probabilities of the singlet ts-DCH and the ss-DCH states are assumed to be the same, because they are expected to be formed through sequential two-photon two-electron ionization. We also calculated the Auger spectra expected in SR experiment, where only the ss-DCH states contribute the Auger spectra because of very low formation probabilities of the ts-DCH states. The result is shown in Fig. S3.

The lower panel of Fig. 8 shows the Auger spectra associated with the C1s core-hole decays, which include the Auger transition from the $C1s^{-2}$ ss-DCH state to the $C1s^{-1}$ CVV states, the transitions from the $C1s^{-1}O1s^{-1}$ ts-DCH states to the $O1s^{-1}$ CVV states, and the transitions from the $C1s^{-1}$ CVV states to the VVVV states. Similarly, the upper panel of Fig. 8 shows the Auger spectra associated with the O1s core-hole decays, including the Auger transition from the $O1s^{-2}$ ss-DCH state to the $O1s^{-1}$ CVV states, the transitions from the $C1s^{-1}O1s^{-1}$ ts-DCH states to the $C1s^{-1}$ CVV states, and the transitions from the $O1s^{-1}$ CVV states to the VVVV states. Since the $O1s^{-1}$ CVV states are generated by the Auger decays of the $O1s^{-2}$ ss-DCH and the $C1s^{-1}O1s^{-1}$ ts-DCH states, the $O1s^{-1}$ CVV $\rightarrow$ VVVV Auger spectrum has two different origins. Likewise, the Auger decays of the $C1s^{-2}$ ss-DCH and the $C1s^{-1}O1s^{-1}$ ts-DCH states contribute to the $C1s^{-1}$ CVV $\rightarrow$ VVVV Auger spectrum. The DCH $\rightarrow$ CVV and CVV $\rightarrow$ VVVV Auger decays of H_2CO involve mainly 6 valence orbitals, i.e., three a_1, one b_1 and two b_2 MOs, because the main valence electron configuration of the DCH states is represented as $(3a_1)^2(4a_1)^2(1b_2)^2(5a_1)^2(1b_1)^2(2b_2)^2$. Since this number of orbitals is larger than those in the CH_4 and NH_3 Auger decays, the discrete

H_2CO Auger intensities in Fig. 8 are more densely distributed in comparison with the intensities for the CH_4 and NH_3 Auger decays. Also, peaks in the convoluted H_2CO Auger spectra are not so distinct as in the spectra of the CH_4 and NH_3 Auger decays.

As shown in the lower panel of Fig. 8, the main part of the C1s^{-2} ss-DCH $\rightarrow$ C1s^{-1} CVV Auger spectrum extends from 270 to 310 eV, with weak intensities around 250 eV. The C1s^{-1}O1s^{-1} ts-DCH $\rightarrow$ O1s^{-1} CVV Auger spectrum, including singlet and triplet contributions, extends from 210 to 250 eV, with weak intensities around 190 eV. The spectrum of the C1s^{-1} CVV $\rightarrow$ VVVV Auger decays extends from 180 to 260 eV. As can be seen in the figure, the Auger spectrum of the C1s^{-2} ss-DCH $\rightarrow$ C1s^{-1} CVV decay is well separated from the other spectra. However, the main parts of the C1s^{-1}O1s^{-1} ts-DCH $\rightarrow$ O1s^{-1} CVV and the C1s^{-1} CVV $\rightarrow$ VVVV Auger spectra overlap each other. The main part of the O1s^{-2} ss-DCH $\rightarrow$ O1s^{-1} CVV Auger spectrum in the upper panel of Fig. 8 extends from 510 to 570 eV, whereas the C1s^{-1}O1s^{-1} ts-DCH $\rightarrow$ C1s^{-1} CVV Auger spectrum extends from 460 to 500 eV. As in the case of the C1s^{-1} core-hole decays, the spectrum of the O1s^{-1} CVV $\rightarrow$ VVVV Auger decay overlaps with those of the C1s^{-1}O1s^{-1} ts-DCH $\rightarrow$ C1s^{-1} CVV Auger spectrum. Our results suggest that the Auger decays of the ss-DCH states may be easily identified in experiment. However, distinction between the ts-DCH $\rightarrow$ CVV Auger spectra and the CVV $\rightarrow$ VVVV Auger spectra may be difficult.

The convoluted C1s^{-2} ss-DCH $\rightarrow$ C1s^{-1} CVV Auger spectrum has two large peaks at 300 eV and 275 eV, and one faint peak at 250 eV. The peak at 300 eV is formed by two-electron vacancy creation in the $5a_1$, $1b_1$, $1b_2$ and $2b_2$ valence MOs, $(5a_1 1b_1 1b_2 2b_2)^{-2}$, while the peak at 275 eV corresponds to the $(3a_1)^{-1}(5a_1 1b_1 1b_2 2b_2)^{-1}$ valence hole creation. The structure between the 300 eV peak and the 275 eV peak involves vacancy creation in the $4a_1$ MO as well. The faint peak at 250 eV is formed by the $(3a_1)^{-2}$ vacancy creation. Note that these assignments are not as obvious as in the cases of the NH_3 and CH_4 Auger spectra. Similarly, we can relate the peaks in the other convoluted Auger spectra to the $(5a_1 1b_1 1b_2 2b_2)^{-2}$, $(3a_1)^{-1}(5a_1 1b_1 1b_2 2b_2)^{-1}$ and $(3a_1)^{-2}$ vacancy creations, with contribution of the $4a_1$ hole creation to the structure between the highest energy and the second highest energy peaks. For example, the peak around 560 eV in the O1s^{-2} ss-DCH $\rightarrow$ O1s^{-1} CVV Auger spectrum and the peaks around 240 eV and 480-490 eV in the C1s^{-1}O1s^{-1} ts-DCH $\rightarrow$ CVV Auger spectra correspond to the $(5a_1 1b_1 1b_2 2b_2)^{-2}$ valence hole creation. Also, the peaks around 530-540 eV in the O1s^{-2} ss-DCH $\rightarrow$ O1s^{-1} CVV Auger spectrum and the peaks around 210-

220 eV and 460-470 eV in the C1s^{-1}O1s^{-1} ts-DCH $\rightarrow$ CVV Auger spectra are formed from the $(3a_1)^{-1}(5a_1 1b_1 1b_2 2b_2)^{-1}$ vacancy creation. The origin of the peaks in the convoluted CVV $\rightarrow$ VVVV Auger spectra were not inspected because these peaks contain too many discrete transitions. Since the shapes of the convoluted CVV $\rightarrow$ VVVV spectra are roughly similar to the DCH $\rightarrow$ CVV Auger spectra, origin of the peaks may be the same as in the DCH $\rightarrow$ CVV Auger spectra.

In the upper panel of Fig. 9, 2D Auger intensity distribution for the C1s^{-2} ss-DCH $\rightarrow$ C1s^{-1} CVV Auger decay and the subsequent C1s^{-1} CVV $\rightarrow$ VVVV Auger decay is shown as functions of the 1st and the 2nd Auger electron kinetic energies. Similarly, 2D Auger spectrum for the O1s^{-2} ss-DCH $\rightarrow$ O1s^{-1} CVV and the O1s^{-1} CVV $\rightarrow$ VVVV Auger decays is shown in the lower panel of Fig. 9. These 2D Auger spectra for the ss-DCH decays may be available in experiment using 4-electron coincidence technique, since the Auger spectra originated from the ss-DCH $\rightarrow$ CVV Auger decays are separated from the other Auger spectra as seen in Fig. 8. Compared to the peaks in the 2D spectra of the CH_4 and NH_3 DCH Auger decays, the peaks in the H_2CO ss-DCH decays look less clear. The highest intensity regions are located around the 1st Auger energies of 295 - 305 eV and the 2nd Auger energies of 220 - 240 eV for the C1s^{-2} case, and around the 1st Auger energies of 550 - 565 eV and the 2nd Auger energies of 470 - 490 eV for the O1s^{-2} case. Location of these highest intensity regions indicates that the $(5a_1 1b_1 1b_2 2b_2)^{-2}$ valence hole creation and subsequent $(5a_1 1b_1 1b_2 2b_2)^{-2}$ valence hole creation are the most probable in the successive two Auger decays. The 2D Auger spectra in Fig. 9 are converted to the 2D intensities as functions of CVV and VVVV binding energies as shown in Fig. 10. Based on these spectra, the highest-intensity peaks can be related to the low-lying CVV and VVVV states. In addition, we can recognize that some CVV states with moderately high energies, 385 eV in the C1s^{-2} case and 640 eV in the O1s^{-2} case, contribute to the higher-intensity peaks in Fig. 10. These 2D intensities as functions of CVV and VVVV binding energies may be available in experiment, if the binding energies of the ss-DCH states as well as the 2D Auger intensities as functions of the 1st and 2nd Auger electron energies are measured.

In the two-step Auger decays of the C1s^{-1}O1s^{-1} ts-DCH states, two different Auger decay pathways exist: (1) the 1st Auger transitions from the ts-DCH states to the O1s^{-1} CVV states, and subsequent Auger transitions from the O1s^{-1} CVV states to the VVVV states, (2) the 1st Auger transitions from the ts-DCH states to the C1s^{-1} CVV states, and

subsequent Auger transitions from the C1s^{-1} CVV states to the VVVV states. In the case (1), the 1st Auger electron has an energy in the region of the C1s core-hole decay and the 2nd Auger energy is in the region of the O1s core-hole decay. In contrast, in the case (2), the 1st Auger electron has an energy in the region of the O1s core-hole decay and the 2nd Auger energy is in the region of the C1s core-hole decay. The 2D Auger intensity distributions originated from these two different Auger decay pathways are shown in the panel (a) and (b) of Fig. 11 as functions of the 1st and 2nd Auger electron energies. It may be difficult in experiment to determine the order of two successive Auger decays, or in other word, to make distinction between these two Auger decay pathways. Thus, two Auger intensities of the case (1) and (2) will not be observed separately, but summation of these two intensities will be measured as shown in the panel (c) of Fig. 11. The highest intensity region is located around the C1s Auger energy of 230 - 240 eV and the O1s Auger energy of 490 eV in the panel (c). As in the cases of the ss-DCH $\rightarrow$ CVV Auger decays, this region roughly corresponds to 4-electron valence vacancy creation in the $5a_1$, $1b_1$, $1b_2$ and $2b_2$ orbitals in the sequential two Auger decays. Although other peaks and structures appear in the 2D intensity distribution, it is difficult to make clear assignment because two different Auger intensities are added in the panel (c). In contrast to the 2D Auger spectra of the ss-DCH decays, the 2D Auger spectrum of the ts-DCH decays in the panel (c) cannot be converted to the intensity as functions of CVV and VVVV binding energies, because such conversion requires individual 2D Auger spectra as in the panels (a) and (b). The integrated 1D Auger spectra as a function of VVVV binding energy, as in the lower panels of Figs. 4 and 7, can be obtained from the 2D spectra in the panels (a) and (b), using the relation $E_{\mathrm{VVVV}} = E_{\mathrm{DCH}} - E_{\mathrm{Auger1}} - E_{\mathrm{Auger2}}$. Because this relation is preserved by exchange of E_{Auger1} and E_{Auger2}, the 1D Auger spectrum can be directly obtained from the 2D spectrum in the panel (c). Thus, if experimental value of E_{DCH} is available, information on VVVV binding energies may be obtained in experimental measurement on the ts-DCH Auger decays.

For reference, ionization energies of the low-lying C1s^{-1} CVV states are shown in Table IV with their main configurations and Auger intensities. Also, the low-lying O1s^{-1} CVV states are listed in Table V. As in the ss-DCH $\rightarrow$ CVV Auger decays of NH_3 and CH_4, the singlet DCH states decay only to the doublet CVV states. In addition to these doublet states, the triplet C1s^{-1}O1s^{-1} ts-DCH states decay to the quartet CVV states as well. In the DCH $\rightarrow$ CVV Auger decays of NH_3 and CH_4, the Auger intensity tends to be larger for

the CVV final ion state with singlet intermediate valence spin than the state with triplet intermediate valence spin. However, this tendency is not obvious in H_2CO.

D. Discussion

Our calculation on NH_3 DCH Auger spectrum has roughly reproduced the experimental Auger spectrum of Eland et al.,[10] and thus similar agreements are expected for CH_4 and H_2CO DCH Auger spectra. The convoluted Auger spectra contain several large distinct peaks, which can be related to two hole creations in valence MOs. In case of the integrated 1D Auger spectra, we can relate their peaks to the electronic configurations of the CVV or VVVV states. Although this kind of assignment can be efficiently performed for small molecules such as CH_4 and NH_3, it may be difficult for larger molecule with many occupied valence MOs.

Since there are many CVV and VVVV states in CH_4,NH_3 and H_2CO, possible number of transitions in the CVV $\rightarrow$ VVVV Auger decays might be huge, and thus distributions of the Auger spectra might be much broader and less structured compared to those of the DCH $\rightarrow$ CVV Auger decays. In contrast to this intuitive expectation, the distributions of the calculated CVV $\rightarrow$ VVVV Auger spectra have similar extent as in the DCH $\rightarrow$ CVV Auger spectra, as can be seen in Figs. 2, 5 and 8. In addition, we can see several distinct peaks in the convoluted CVV $\rightarrow$ VVVV Auger spectra, which is especially pronounced in the CH_4 case. Our results can be understood in the following manner. When we evaluated the DCH $\rightarrow$ CVV Auger intensities using Eqs. (1) and (6), we approximated the DCH state by a single CSF function. This means that the DCH $\rightarrow$ CVV Auger intensity is noticeably large only when the CI wave function of the CVV state is dominated by a configuration obtained by removing two valence electrons from and adding one core electron to the DCH configuration, because only such a configuration has non-zero Auger amplitude in Eq. (1). Similarly, the CVV $\rightarrow$ VVVV Auger intensity is noticeably large only when (1) the CVV state has large intensity in the DCH $\rightarrow$ CVV Auger decay and (2) the CI wave function of the VVVV state is dominated by a configuration obtained by removing two valence electrons from and adding one core electron to the main configuraton of the CVV state. This also means that the final VVVV ion states are all dominated by electronic configurations constructed from the occupied valence MOs of the DCH state. The above conditions (1) and (2) severely

restrict possible pairs of CVV and VVVV states which have large contribution to the CVV $\rightarrow$ VVVV Auger decay. The distribution of the CVV $\rightarrow$ VVVV Auger spectra cannot be as broad as intuitively expected from the distribution of the CVV and VVVV binding energies, because of the selection conditions stated above. These conditions also indicate that the Auger electron kinetic energy in the CVV $\rightarrow$ VVVV Auger decay is related to the two-electron valence hole creation in the occupied MOs of the DCH state. In other word, the CVV $\rightarrow$ VVVV Auger intensity can be noticeably large only around the specific energy region related to the two-electron valence hole creation, although this property may be less pronounced as number of occupied MOs increases.

The total intensity of the H_2CO ts-DCH $\rightarrow$ C1s^{-1} CVV Auger transitions, obtained by integrating the spectrum by the Auger kinetic energy, is larger than that of the H_2CO ts-DCH $\rightarrow$ O1s^{-1} CVV Auger transitions, as seen in Fig. 8. This difference indicates that the occupied valence MOs of the ts-DCH states have larger overlap with the oxygen site than that with the carbon site. If individual, separated experimental spectra are available for ts-DCH $\rightarrow$ CVV, ss-DCH $\rightarrow$ CVV and CVV $\rightarrow$ VVVV Auger transitions of H_2CO, and if assignment of peaks is available in terms of the occupied valence MOs, we can compare intensities of peaks having the same MO assignment in different Auger transitions. Such comparison may be useful in understanding relaxation of the valence MOs and overlap of MOs with different atomic sites. Similar analysis for ss- and ts-DCH Auger decays of other molecules will be interesting, if experimental measurement is possible.

In this work, the Wentzel's ansatz was employed to estimate intensities of the 1st Auger transition from DCH to CVV states, and of the 2nd Auger transition from CVV to VVVV states. This means that we assume a "three-step" model in which DCH state creation by photoionization, the 1st Auger decay, and the 2nd Auger decay are all treated independently, as in the two-step model of single core-hole Auger decay.[30,45–47] This assumption is valid when the lifetimes of the intermediate states, DCH and CVV states in this case, are sufficiently long that the interaction between photoelectron and the 1st Auger electron as well as the interaction between the 1st Auger electron and the 2nd Auger electron are negligibly small. According to the multiconfiguration Dirac-Fock calculation by Chen on atomic DCH state,[16] the Auger transition rates of DCH states for the low-Z elements are much larger than the Auger rates of SCH states; in the case of neon, the Auger rate per K hole of the DCH state is about 42 % larger than the rate of the SCH state. The Auger lifetimes of the CH_4, NH_3

and H_2CO DCH states may also be short, but such values are not known so far. Thus, it will be interesting as well as necessary to verify the validity of the "three-step" assumption in future, for example, by performing calculation or experimental measurement on lifetime of DCH and CVV states, or by measuring angular distribution of Auger electrons in the molecular-frame as in the SCH Auger process.[45,47]

Following Mitani et al.,[29] we approximated two-electron integrals in Eq. (6), which involve core-hole, valence and Auger continuum orbitals, by the Löwdin population of the valence MO in the integral. When an Auger transition amplitude is dominated by a pair of CSFs, one in the initial state and the other in the final state, this approximation may be valid as demonstrated by Mitani et al.[29] However, when more than one pair of CSFs equally contributes to an Auger amplitude, this approximation can be less accurate because it does not necessarily preserve proper relative phases of two-electron integrals in the Auger amplitude. In our calculation, Auger amplitudes were dominated by one pair of CSFs in most cases and thus this approximation is expected to be valid. Still, refinement of this approximation is desirable.

In this paper, we have studied basic properties of molecular DCH Auger decay by estimating Auger spectra originated from the normal Auger decays of the molecular DCH states. Angular distribution of the Auger electron was not studied in this work, though the experimental measurement has already been performed for the Auger decay of the N_2 ss-DCH state.[9] Angular distribution of the Auger electron may contain additional information on valence holes created in DCH or CVV Auger decays, and will be an interesting subject for theoretical study in future. In addition to the normal Auger decay of molecular DCH state, the Auger decays of doubly core excited resonance state and shake-up satellite state have been studied experimentally[10,11] and may deserve further theoretical study as well.

At this point of time, experimental Auger spectra are only available for the Auger decay of ss-DCH state.[8,10,11] However, the XFEL experiment on CO molecule has been performed at LCLS and the Auger spectra of the ts-DCH decay are being analyzed.[48] Thus, we can expect further experimental information in this subject in the near future.

IV. SUMMARY

We have performed theoretical investigation on Auger decay of molecular DCH state, for which experimental information becomes available for several molecules recently. Assuming sequential two-step Auger transitions from DCH state to CVV states and from CVV states to VVVV states, Auger electron kinetic energy distributions were estimated for CH_4, NH_3 and H_2CO molecules based on the CASSCF and CASCI calculations. The Auger spectra of the CH_4 and NH_3 ss-DCH Auger decays contain two well separated components: one from the 1st Auger transition from the DCH state to the CVV states and the other from the 2nd Auger transition from the CVV states to the VVVV final ion states. Our result roughly agrees with the experimental Auger spectra of NH_3 ss-DCH decay,[10] but experimental spectrum with better energy resolution is desired for precise comparison. The calculated Auger spectrum of H_2CO DCH decay has more complicated structure compared to the spectra of CH_4 and NH_3 DCH decays, due to existence of the ts-DCH Auger decay. In the Auger spectrum of H_2CO DCH decay, the components originated from the ss-DCH $\rightarrow$ CVV Auger decays are well separated from the rest of the spectrum. However, the components originated from the ts-DCH $\rightarrow$ CVV Auger decays, and the components from the CVV $\rightarrow$ VVVV Auger decays overlap each other, making separation of the spectra difficult. The 2D Auger spectrum may be helpful in resolving this difficulty. We hope our calculation and analysis on the results, especially the H_2CO DCH Auger spectrum, will be useful in interpreting experimental result expected in the near future.

ACKNOWLEDGMENTS

We thank E.H.D. Eland for sending us the experimental Auger spectrum of the NH_3 DCH Auger decays. M.T. also thank N. Kosugi for discussion on theoretical method. M.E. acknowledge the support from JST-CREST and a Grant-in-Aid for Scientific Research from the JSPS.

REFERENCES

[1]L. S. Cederbaum, F. Tarantelli , A. Sgamellotti, and J. Schirmer, J. Chem. Phys. **85**, 6513 (1986).

[2]L. S. Cederbaum, F. Tarantelli, A. Sgamellotti, and J. Schirmer, J. Chem. Phys. **86**, 2168 (1987).

[3]H. Agren and H. J. A. Jensen, Chem. Phys. **172**, 45 (1993).

[4]R. Santra, N. V. Kryzhevoi, and L. S. Cederbaum, Phys. Rev. Lett. **103**, 013002 (2009).

[5]M. Tashiro, M. Ehara, H. Fukuzawa, K. Ueda, C. Buth, N. V. Kryzhevoi, and L. S. Cederbaum, J. Chem. Phys. **132**, 184302 (2010).

[6]M. Tashiro, M. Ehara, and K. Ueda, Chem. Phys. Lett. **496**, 217 (2010).

[7]N. V. Kryzhevoi, R. Santra, and L. S. Cederbaum, J. Chem. Phys. **135**, 084302 (2011).

[8]L. Fang, M. Hoener, O. Gessner, F. Tarantelli, S. T. Pratt, O. Kornilov, C. Buth, M. Guehr, E. P. Kanter, C. Bostedt, J. D. Bozek, P. H. Bucksbaum, M. Chen, R. Coffee, J. Cryan, M. Glownia, E. Kukk, S. R. Leone, and N. Berrah, Phys. Rev. Lett. **105**, 083005 (2010).

[9]J. P. Cryan, J. M. Glownia, J. Andreasson, A. Belkacem, N. Berrah, C. I. Blaga, C. Bostedt, J. Bozek, C. Buth, L. F. DiMauro, L. Fang, O. Gessner, M. Guehr, J. Hajdu, M. P. Hertlein, M. Hoener, O. Kornilov, J. P. Marangos, A. M. March, B. K. McFarland, H. Merdji, V. S. Petrovic, C. Raman, D. Ray, D. Reis, F. Tarantelli, M. Trigo, J. L. White, W. White, L. Young, P. H. Bucksbaum, and R. N. Coffee, Phys. Rev. Lett. **105**, 083004 (2010).

[10]J. H. D. Eland, M. Tashiro, P. Linusson, M. Ehara, K. Ueda, and R. Feifel, Phys. Rev. Lett. **105**, 213005 (2010).

[11]P. Lablanquie, F. Penent, J. Palaudoux, L. Andric, P. Selles, S. Carniato, K. Bucar, M. Zitnik, M. Huttula, J. H. D. Eland, E. Shigemasa, K. Soejima, Y. Hikosaka, I. H. Suzuki, M. Nakano, and K. Ito, Phys. Rev. Lett. **106**, 063003 (2011).

[12]O. Takahashi, M. Tashiro, M. Ehara, K. Yamasaki, and K. Ueda, Chem. Phys. **384**, 28 (2011).

[13]P. Emma, R. Akre, J. Arthur, R. Bionta, C. Bostedt, J. Bozek, A. Brachmann, P. Bucksbaum, R. Coffee, F. J. Decker, Y. Ding, D. Dowell, S. Edstrom, A. Fisher, J. Frisch, S. Gilevich, J. Hastings, G. Hays, P. Hering, Z. Huang, R. Iverson, H. Loos, M. Messerschmidt, A. Miahnahri, S. Moeller, H. D. Nuhn, G. Pile, D. Ratner, J. Rzepiela, D. Schultz, T. Smith, P. Stefan, H. Tompkins, J. Turner, J. Welch, W. White, J. Wu, G. Yocky, and

J. Galayda, Nat. Photon. **4**, 641 (2010).

[14]B. W. J. McNeil and N. R. Thompson, Nat. Photon. **4**, 814 (2010).

[15]P. Linusson, O. Takahashi, K. Ueda, J. H. D. Eland, and R. Feifel, Phys. Rev. A **83**, 022506 (2011).

[16]M. H. Chen, Phys. Rev. A **44**, 239 (1991).

[17]T. A. Carlson and M. O. Krause, Phys. Rev. Lett. **14**, 390 (1965).

[18]M. Y. Amusia, I. S. Lee, and V. A. Kilin, Phys. Rev. A **45**, 4576 (1992).

[19]K. Faegri and H. P. Kelly, Phys. Rev. A **19** (1979).

[20]M. Higashi, E. Hiroike, and T. Nakajima, Chem. Phys. **68**, 377 (1982).

[21]R. Colle and S. Simonucci, Phys. Rev. A **39**, 6247 (1989).

[22]K. Zahringer, H. D. Meyer, and L. S. Cederbaum, Phys. Rev. A **45**, 318 (1992).

[23]H. Siegbahn, L. Asplund, and P. Kelfve, Chem. Phys. Lett. **35**, 330 (1975).

[24]R. Fink, J. Electron Spectrosc. Relat. Phenom. **76**, 295 (1995).

[25]V. Carravetta and H. Agren, Phys. Rev. A **35**, 1022 (1987).

[26]D. E. Ramaker, J. S. Murday, N. H. Turner, G. Moore, M. G. Lagally, and J. Houston, Phys. Rev. B **19**, 5375 (1979).

[27]F. Tarantelli, A. Sgamellotti, and L. S. Cederbaum, J. Chem. Phys. **94**, 523 (1991).

[28]T. R. Walsh, T. E. Meehan, and F. P. Larkins, J. Phys. B **27**, 2211 (1994).

[29]M. Mitani, O. Takahashi, K. Saito, and S. Iwata, J. Electron Spectrosc. Relat. Phenom. **128**, 103 (2003).

[30]H. Agren, A. Cesar, and C. M. Liegener, Adv. Quantum Chem. **23**, 1 (1992).

[31]G. Wentzel, Z. Phys. **43**, 524 (1927).

[32]F. P. Larkins, J. Electron Spectrosc. Relat. Phenom. **51**, 115 (1990).

[33]N. Kosugi, Chem. Phys. **289**, 117 (2003).

[34]N. N. Greenwood and A. Earnshaw, *Chemistry of the Elements, 2nd Edition* (Butterworth-Heinemann, Oxford, 1997).

[35]D. L. Gray and A. G. Robiette, Mol. Phys. **37**, 1901 (1979).

[36]T. Oka, J. Phys. Soc. Jpn. **15**, 2274 (1960).

[37]P. J. Knowles and H.-J. Werner, Chem. Phys. Lett. **115**, 259 (1985).

[38]H.-J. Werner and P. J. Knowles, J. Chem. Phys. **82**, 5053 (1985).

[39]T. H. Dunning, Jr., J. Chem. Phys. **90**, 1007 (1989).

[40]H.-J. Werner, P. J. Knowles, F. R. Manby, M. Schütz, P. Celani, G. Knizia, T. Korona, R. Lindh, A. Mitrushenkov, G. Rauhut, T. B. Adler, R. D. Amos, A. Bernhardsson, A. Berning, D. L. Cooper, M. J. O. Deegan, A. J. Dobbyn, F. Eckert, E. Goll, C. Hampel, A. Hesselmann, G. Hetzer, T. Hrenar, G. Jansen, C. Köppl, Y. Liu, A. W. Lloyd, R. A. Mata, A. J. May, S. J. McNicholas, W. Meyer, M. E. Mura, A. Nicklass, P. Palmieri, K. Pflüger, R. Pitzer, M. Reiher, T. Shiozaki, H. Stoll, A. J. Stone, R. Tarroni, T. Thorsteinsson, M. Wang, and A. Wolf, "Molpro, version 2010.1, a package of ab initio programs," (2010).

[41]L. A. Morgan, J. Tennyson, and C. J. Gillan, Comput. Phys. Commun. **114**, 120 (1998).

[42]See supplementary material at http://dx.doi.org/XXX for effect of number of CI coefficients included in the calculation (Fig. S1), effect of FWHM Gaussian width on the CH_4 Auger spectrum (Fig. S2), and the theoretical H_2CO Auger spectra for SR experiment (Fig. S3).

[43]P. S. Bagus, M. Schrenk, D. W. Davis, and D. A. Shirley, Phys. Rev. A **9**, 1090 (1974).

[44]D. Di Tommaso and P. Decleva, J. Chem. Phys. **123**, 064311 (2005).

[45]R. Guillemin, E. Shigemasa, K. Le Guen, D. Ceolin, C. Miron, N. Leclercq, P. Morin, and M. Simon, Phys. Rev. Lett. **87**, 203001 (2001).

[46]T. Weber, M. Weckenbrock, M. Balser, L. Schmidt, O. Jagutzki, W. Arnold, O. Hohn, M. Schoffler, E. Arenholz, T. Young, T. Osipov, L. Foucar, A. De Fanis, R. Muino, H. Schmidt-Bocking, C. Cocke, M. Prior, and R. Dorner, Phys. Rev. Lett. **90**, 153003 (2003).

[47]G. Pruemper, H. Fukuzawa, D. Rolles, K. Sakai, K. C. Prince, J. R. Harries, Y. Tamenori, N. Berrah, and K. Ueda, Phys. Rev. Lett. **101**, 233202 (2008).

[48]N. Berrah, L. Fang, B. Murphy, T. Osipov, K. Ueda, E. Kukk, R. Feifel, P. van der Meulen, P. Salen, H. Schmidt, R. Thomas, M. Larsson, R. Richter, K. Prince, J. Bozek, C. Bostedt, S. Wada, M. N. Piancastelli, M. Tashiro, and M. Ehara, Proc. Natl Acad. Sci. USA in press.

LIST OF FIGURES

1 An example of two-step Auger decays originated from the ss-DCH state of NH_3. Thin black arrows represent displacements of electrons during the Auger decays. In the 1st Auger decay, the CVV state with one vacancy in the $3a_1$ orbital and another vacancy in the $1e$ orbital is produced. Then in the 2nd Auger transition, this CVV state decays to produce the VVVV state with additional vacancies in the $1e$ and $2a_1$ orbitals. 31

2 Calculated intensities of the Auger decays of the CH_4 C1s^{-2} DCH state (DCH→CVV) and the C1s^{-1} CVV states (CVV→VVVV), as a function of Auger electron kinetic energy. The vertical full lines represent the discrete Auger spectrum obtained by the CASCI wave functions with the frozen orbital approximation. The dashed lines are obtained by convoluting the discrete Auger intensities with Gaussian function having 4.5 eV width. 32

3 (Upper panel) Two-dimensional (2D) intensity of the two-step Auger decays of the CH_4 C1s^{-2} ss-DCH state, as functions of kinetic energies of the 1st and the 2nd Auger electrons. The 1st electrons are emitted by the Auger transition from the C1s^{-2} DCH state to the C1s^{-1} CVV states, and the 2nd electrons are emitted by the transition from the C1s^{-1} CVV states to the VVVV states. This 2D spectrum represents a probability of finding two Auger electrons at specific pair of energies. (Lower panel) 2D Auger intensity as functions of CVV and VVVV binding energies, converted from the 2D spectrum in the upper panel. These intensities were obtained by smoothing calculated discrete Auger intensities, as in the convoluted intensities in Fig. 2. Unit of the intensity is arbitrary. 33

4 Integrated 1D Auger intensities as a function of CVV binding energy (upper panel) and VVVV binding energy (lower panel). These spectra can be obtained by integrating the 2D Auger spectrum in the lower panel of Fig. 3 by VVVV energy (upper panel) or CVV energy (lower panel). The vertical bars represent original theoretical intensities which can be directly obtained from our calculation. The other details are the same as in Fig. 2. 34

5 Calculated and experimental Auger intensities of the NH_3 core-hole decays as a function of Auger electron kinetic energy. DCH→CVV: the transition from the $N1s^{-2}$ DCH state to the $N1s^{-1}$ CVV states, CVV→VVVV: the transition from the $N1s^{-1}$ CVV states to the VVVV states, SCH→VV: the Auger decay of the $N1s^{-1}$ SCH state. Expt.:experimental Auger spectrum of Eland et al.[10]. The other details are the same as in Fig. 2. 35

6 (Upper panel) 2D intensity of the two-step Auger decays of the NH_3 $N1s^{-2}$ DCH state, as functions of kinetic energies of the 1st and the 2nd Auger electrons. (Lower panel) 2D Auger intensity as functions of CVV and VVVV binding energies, converted from the 2D spectrum in the upper panel. The other details are the same as in Fig. 3. 36

7 Integrated 1D Auger intensities as a function of CVV binding energy (upper panel) and VVVV binding energy (lower panel), obtained by integrating the 2D Auger spectrum in the lower panel of Fig. 6. The other details are the same as in Fig. 4. 37

8 (Upper panel) The Auger intensities for the O1s core-hole decays of H_2CO molecule, which include the Auger decays of the H_2CO $O1s^{-2}$ ss-DCH state, the $C1s^{-1}O1s^{-1}$ ts-DCH states, and the $O1s^{-1}$ CVV states. (Lower panel) The Auger intensities for the C1s core-hole decays of H_2CO molecule, which include the Auger decays of the H_2CO $C1s^{-2}$ ss-DCH state, the $C1s^{-1}O1s^{-1}$ ts-DCH states, and the $C1s^{-1}$ CVV states. The other details are the same as in Fig. 2. 38

9 (Upper panel) 2D intensity of the two-step Auger decays of the H_2CO $C1s^{-2}$ ss-DCH state, as functions of kinetic energies of the 1st and the 2nd Auger electrons. (Lower panel) 2D intensity of the two-step Auger decays of the H_2CO $O1s^{-2}$ ss-DCH state, as functions of kinetic energies of the 1st and the 2nd Auger electrons. The other details are the same as in Fig. 3. 39

10 (Upper panel) 2D Auger intensity of the H_2CO $C1s^{-2}$ ss-DCH decay as functions of CVV and VVVV binding energies, converted from the 2D spectrum in the upper panel of Fig. 9. (Lower panel) 2D Auger intensity of the H_2CO $O1s^{-2}$ ss-DCH decay as functions of CVV and VVVV binding energies, converted from the 2D spectrum in the lower panel of Fig. 9. The other details are the same as in Fig. 3. 40

11 2D Auger spectra of the two-step Auger decays of the H_2CO $C1s^{-1}O1s^{-1}$ ts-DCH states. Panel (a): 2D spectrum with the 1st Auger transitions from the $C1s^{-1}O1s^{-1}$ state to the $C1s^{-1}$ CVV states and the 2nd transitions from the $C1s^{-1}$ CVV states to the VVVV states. Panel (b): 2D spectrum with the 1st Auger transitions from the $C1s^{-1}O1s^{-1}$ state to the $O1s^{-1}$ CVV states and the 2nd transitions from the $O1s^{-1}$ CVV states to the VVVV states. Panel (c): 2D Auger intensity as functions of C1s and O1s Auger electron energies, obtained by adding the intensities of two different Auger decay pathways in the panel (a) and (b). 41

S1 Effect of number of CI coefficients included in the calculation. We performed the same calculation as in Fig. 2, but with 30 configurations with the largest CI coefficients. The result is very similar to the CH_4 DCH Auger spectra in Fig. 2 which were calculated with 5 configurations with the largest CI coefficients. The details of the figure is the same as in the Fig. 2. 42

S2 Effect of Gaussian width used for convolution. The convoluted CH_4 DCH Auger spectra with different FWHM width are shown. Our result suggests that FWHM has strong influence on the shape of the Auger spectra, which may be important when we compare calculated spectrum with experimental result. The details of the figure is the same as in Fig. 2. 43

S3 H_2CO DCH $\rightarrow$ CVV and CVV $\rightarrow$ VVVV Auger spectra expected in SR experiment. In Fig. 8, we show H_2CO DCH Auger spectra expected for XFEL experiment. In case of SR experiment, formation efficiencies of the ts-DCH states are expected to be low, 1/100 of the ss-DCH states. Thus, we can ignore the ts-DCH contributions in simulating Auger spectra in SR experiment. In this figure, the Auger spectra without the ts-DCH contribution is shown. The details of the figure is the same as in Fig. 8. 44

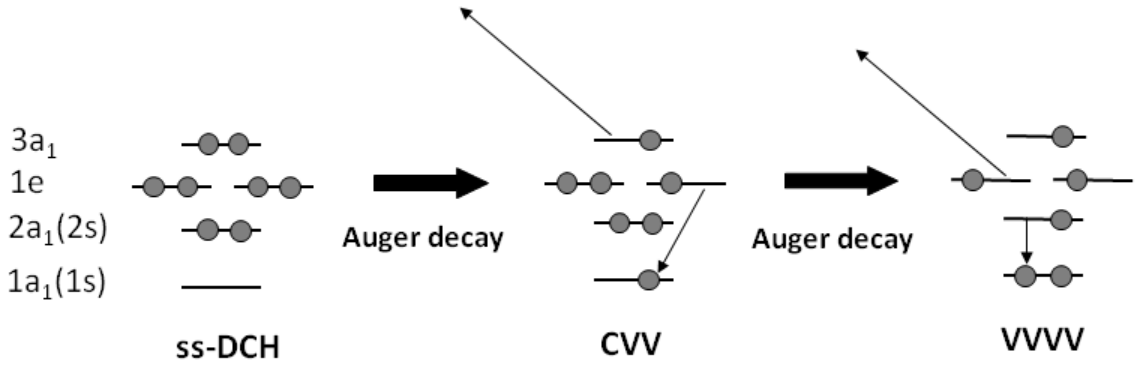

FIG. 1. An example of two-step Auger decays originated from the ss-DCH state of NH_3. Thin black arrows represent displacements of electrons during the Auger decays. In the 1st Auger decay, the CVV state with one vacancy in the $3a_1$ orbital and another vacancy in the $1e$ orbital is produced. Then in the 2nd Auger transition, this CVV state decays to produce the VVVV state with additional vacancies in the $1e$ and $2a_1$ orbitals.

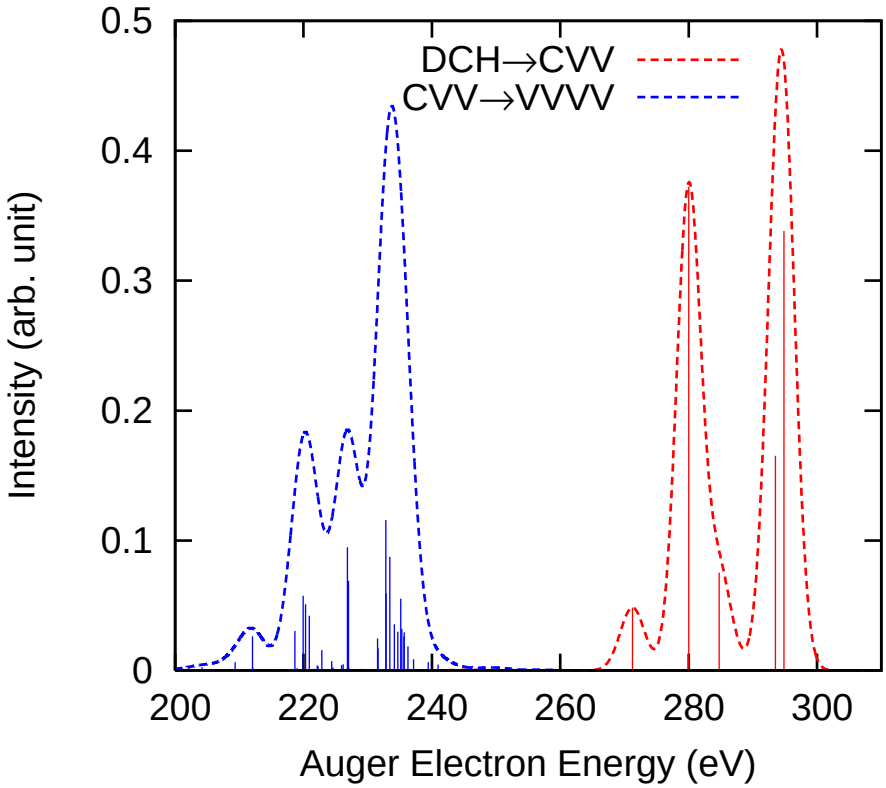

FIG. 2. Calculated intensities of the Auger decays of the CH_4 $C1s^{-2}$ DCH state (DCH→CVV) and the $C1s^{-1}$ CVV states (CVV→VVVV), as a function of Auger electron kinetic energy. The vertical full lines represent the discrete Auger spectrum obtained by the CASCI wave functions with the frozen orbital approximation. The dashed lines are obtained by convoluting the discrete Auger intensities with Gaussian function having 4.5 eV width.

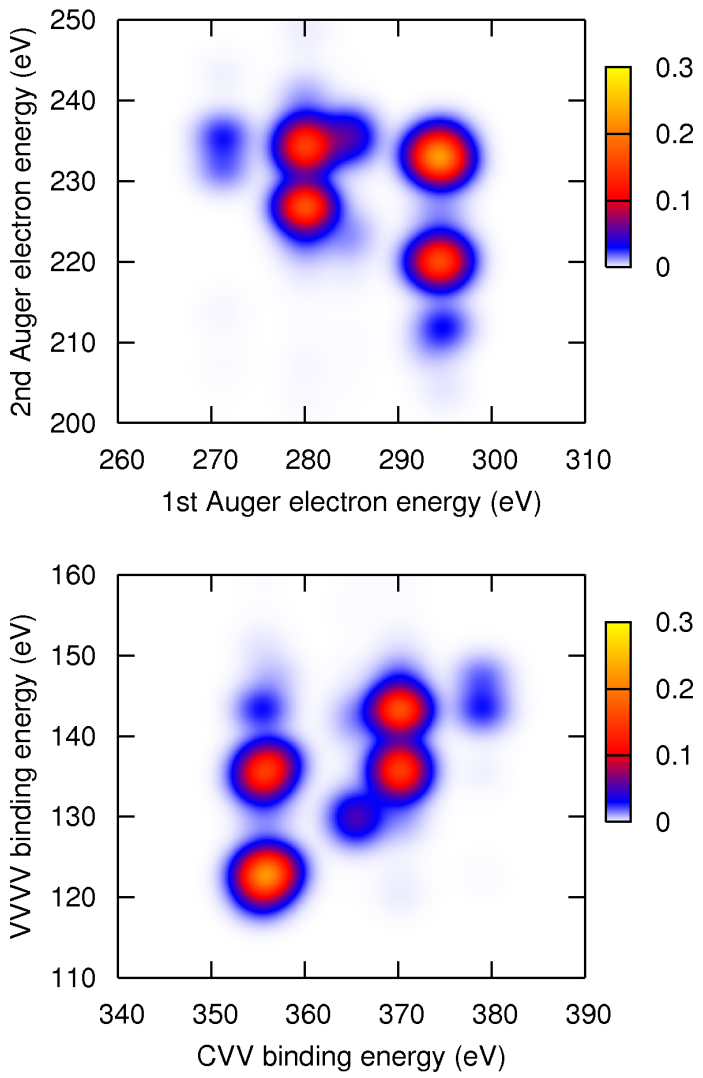

FIG. 3. (Upper panel) Two-dimensional (2D) intensity of the two-step Auger decays of the CH_4 $C1s^{-2}$ ss-DCH state, as functions of kinetic energies of the 1st and the 2nd Auger electrons. The 1st electrons are emitted by the Auger transition from the $C1s^{-2}$ DCH state to the $C1s^{-1}$ CVV states, and the 2nd electrons are emitted by the transition from the $C1s^{-1}$ CVV states to the VVVV states. This 2D spectrum represents a probability of finding two Auger electrons at specific pair of energies. (Lower panel) 2D Auger intensity as functions of CVV and VVVV binding energies, converted from the 2D spectrum in the upper panel. These intensities were obtained by smoothing calculated discrete Auger intensities, as in the convoluted intensities in Fig. 2. Unit of the intensity is arbitrary.

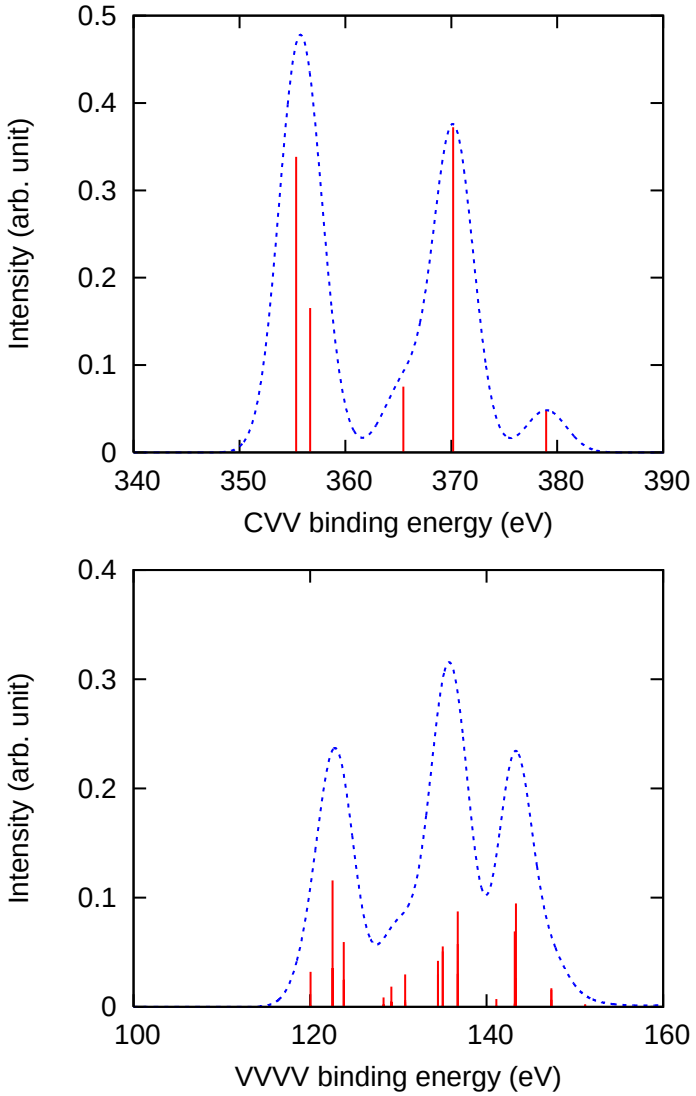

FIG. 4. Integrated 1D Auger intensities as a function of CVV binding energy (upper panel) and VVVV binding energy (lower panel). These spectra can be obtained by integrating the 2D Auger spectrum in the lower panel of Fig. 3 by VVVV energy (upper panel) or CVV energy (lower panel). The vertical bars represent original theoretical intensities which can be directly obtained from our calculation. The other details are the same as in Fig. 2.

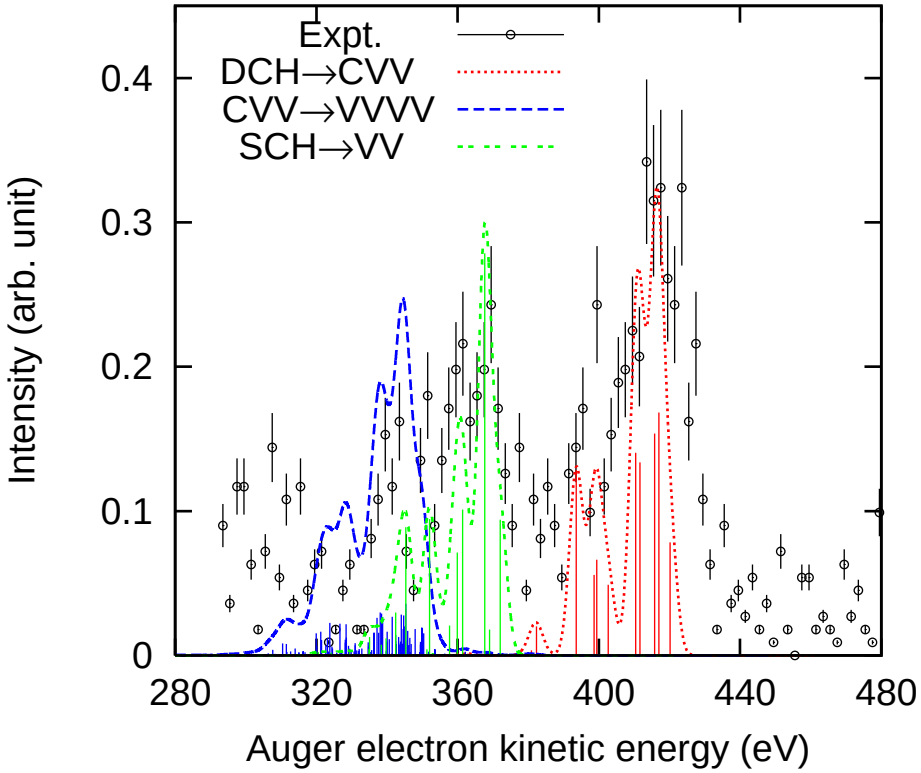

FIG. 5. Calculated and experimental Auger intensities of the NH_3 core-hole decays as a function of Auger electron kinetic energy. DCH→CVV: the transition from the $N1s^{-2}$ DCH state to the $N1s^{-1}$ CVV states, CVV→VVVV: the transition from the $N1s^{-1}$ CVV states to the VVVV states, SCH→VV: the Auger decay of the $N1s^{-1}$ SCH state. Expt.:experimental Auger spectrum of Eland et al.[10]. The other details are the same as in Fig. 2.

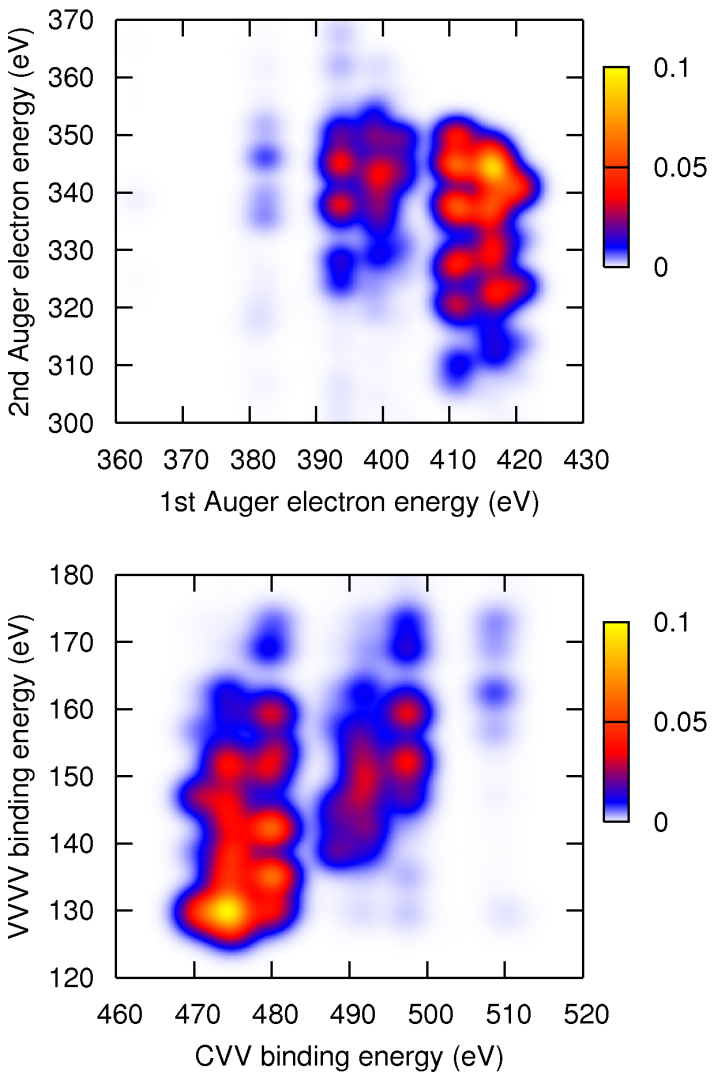

FIG. 6. (Upper panel) 2D intensity of the two-step Auger decays of the NH_3 N1s^{-2} DCH state, as functions of kinetic energies of the 1st and the 2nd Auger electrons. (Lower panel) 2D Auger intensity as functions of CVV and VVVV binding energies, converted from the 2D spectrum in the upper panel. The other details are the same as in Fig. 3.

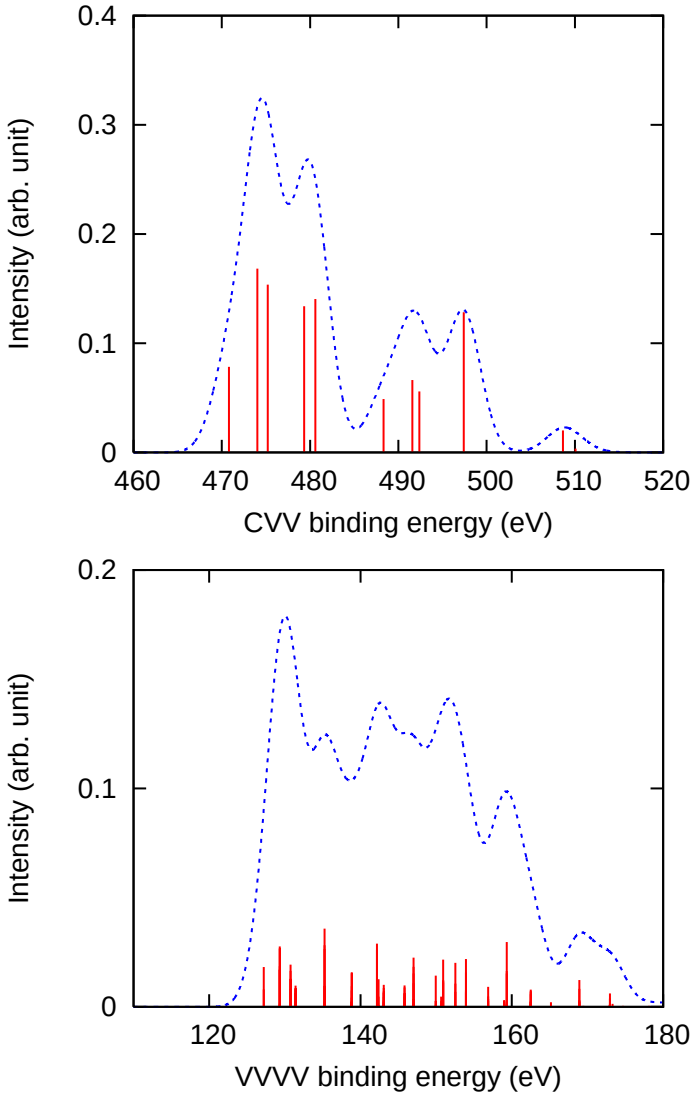

FIG. 7. Integrated 1D Auger intensities as a function of CVV binding energy (upper panel) and VVVV binding energy (lower panel), obtained by integrating the 2D Auger spectrum in the lower panel of Fig. 6. The other details are the same as in Fig. 4.

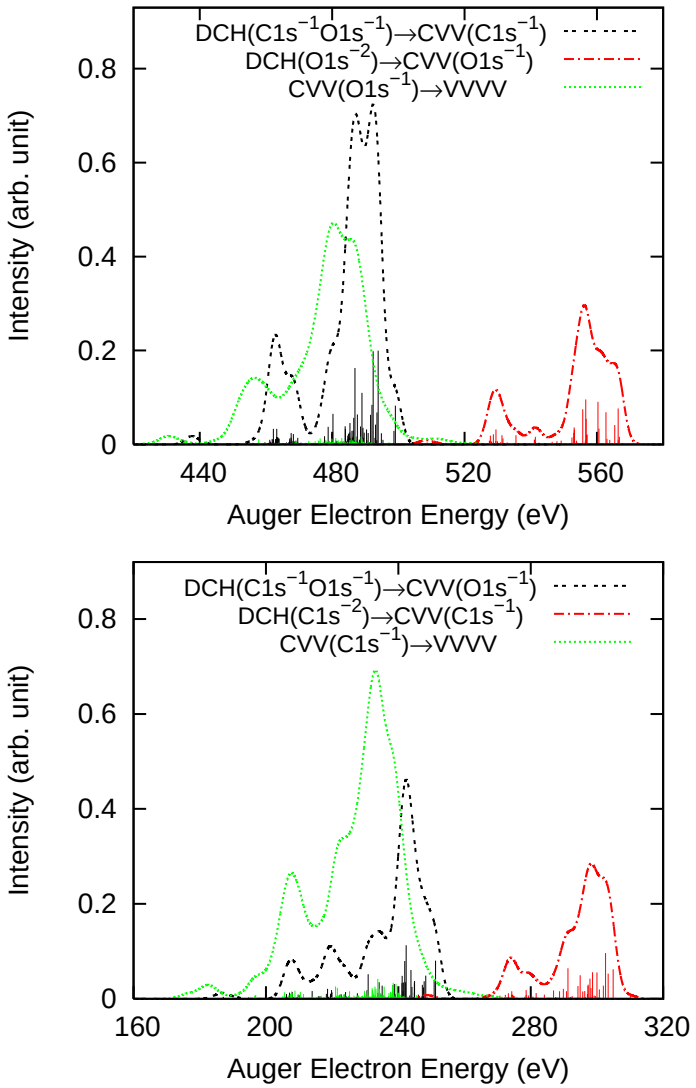

FIG. 8. (Upper panel) The Auger intensities for the O1s core-hole decays of H_2CO molecule, which include the Auger decays of the H_2CO O1s^{-2} ss-DCH state, the C1s^{-1}O1s^{-1} ts-DCH states, and the O1s^{-1} CVV states. (Lower panel) The Auger intensities for the C1s core-hole decays of H_2CO molecule, which include the Auger decays of the H_2CO C1s^{-2} ss-DCH state, the C1s^{-1}O1s^{-1} ts-DCH states, and the C1s^{-1} CVV states. The other details are the same as in Fig. 2.

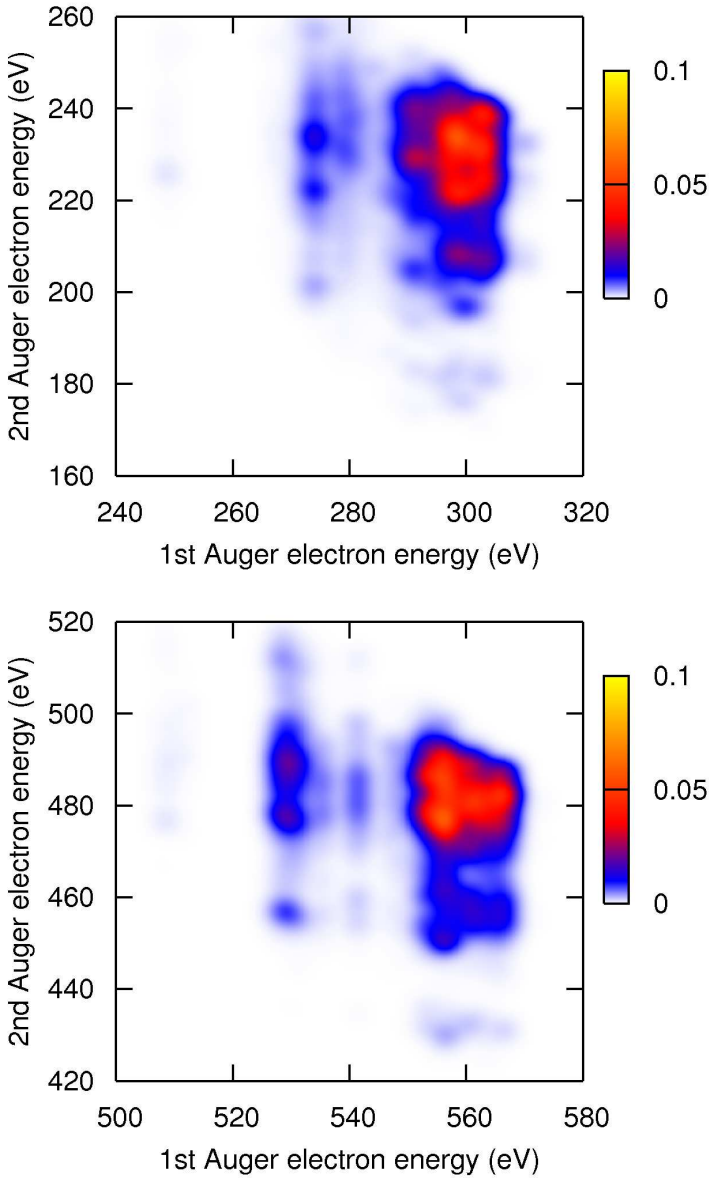

FIG. 9. (Upper panel) 2D intensity of the two-step Auger decays of the H_2CO C1s^{-2} ss-DCH state, as functions of kinetic energies of the 1st and the 2nd Auger electrons. (Lower panel) 2D intensity of the two-step Auger decays of the H_2CO O1s^{-2} ss-DCH state, as functions of kinetic energies of the 1st and the 2nd Auger electrons. The other details are the same as in Fig. 3.

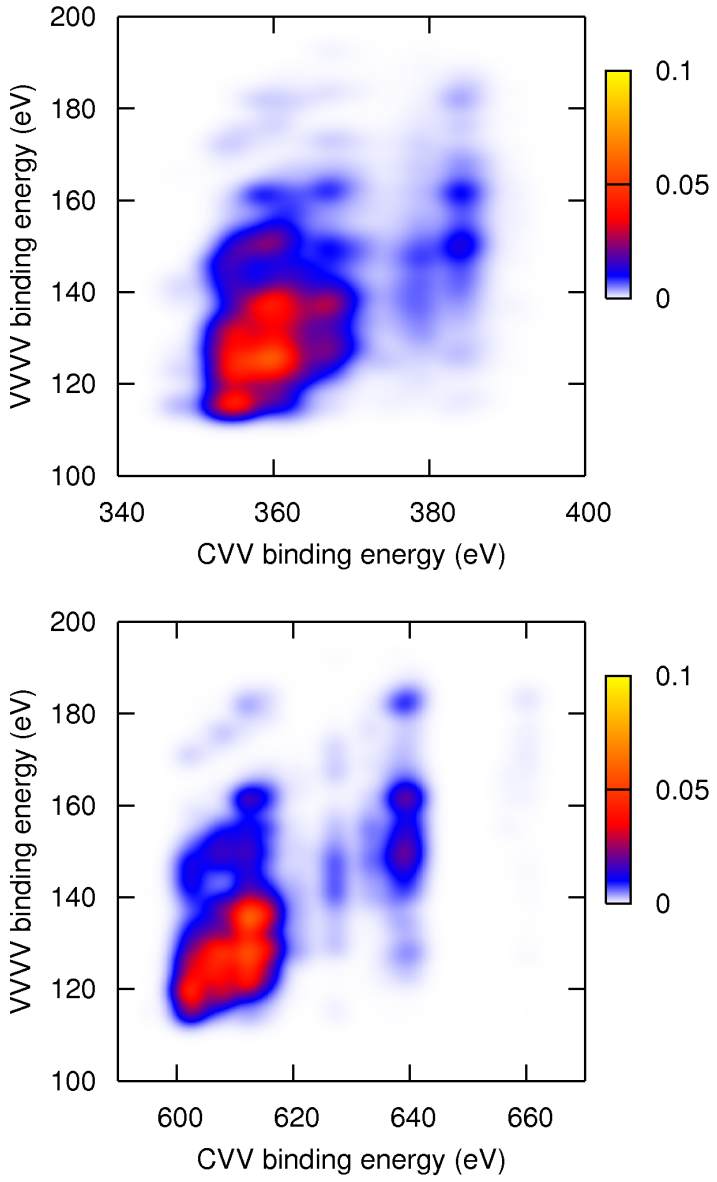

FIG. 10. (Upper panel) 2D Auger intensity of the H_2CO C1s^{-2} ss-DCH decay as functions of CVV and VVVV binding energies, converted from the 2D spectrum in the upper panel of Fig. 9. (Lower panel) 2D Auger intensity of the H_2CO O1s^{-2} ss-DCH decay as functions of CVV and VVVV binding energies, converted from the 2D spectrum in the lower panel of Fig. 9. The other details are the same as in Fig. 3.

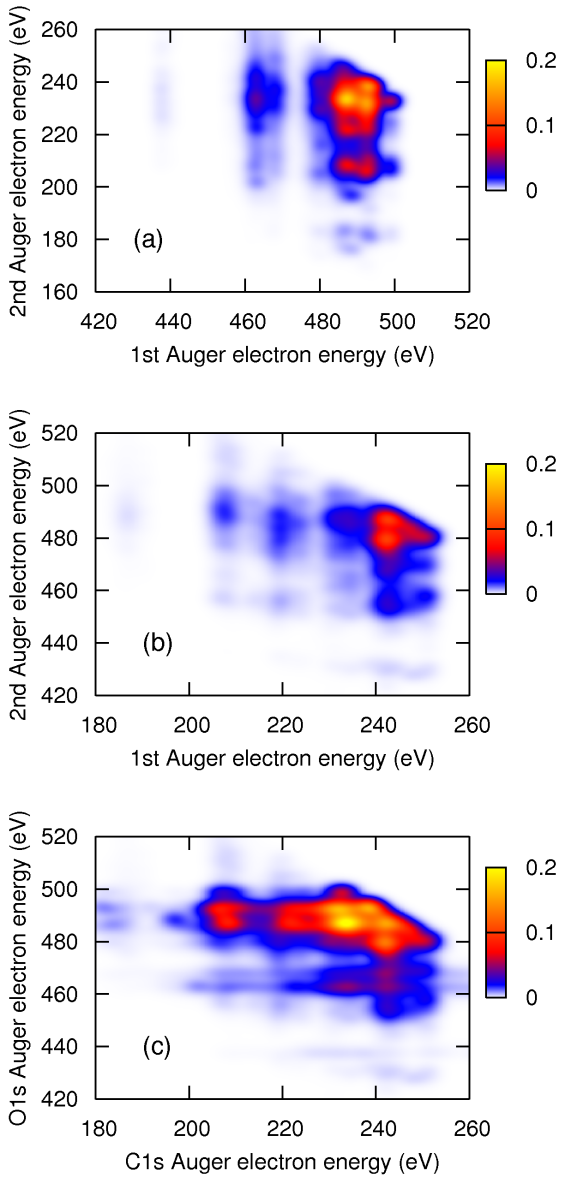

FIG. 11. 2D Auger spectra of the two-step Auger decays of the H_2CO $C1s^{-1}O1s^{-1}$ ts-DCH states. Panel (a): 2D spectrum with the 1st Auger transitions from the $C1s^{-1}O1s^{-1}$ state to the $C1s^{-1}$ CVV states and the 2nd transitions from the $C1s^{-1}$ CVV states to the VVVV states. Panel (b): 2D spectrum with the 1st Auger transitions from the $C1s^{-1}O1s^{-1}$ state to the $O1s^{-1}$ CVV states and the 2nd transitions from the $O1s^{-1}$ CVV states to the VVVV states. Panel (c): 2D Auger intensity as functions of C1s and O1s Auger electron energies, obtained by adding the intensities of two different Auger decay pathways in the panel (a) and (b).

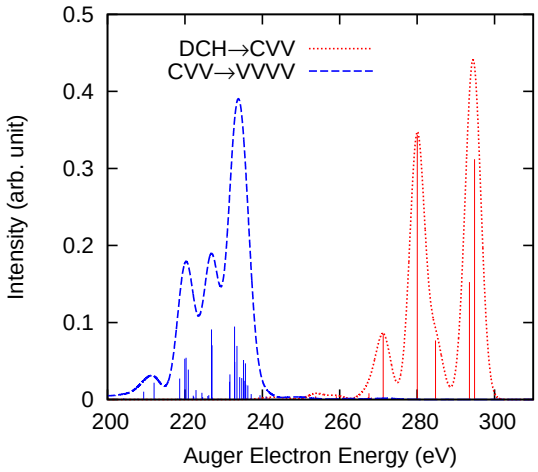

FIG. S1. Effect of number of CI coefficients included in the calculation. We performed the same calculation as in Fig. 2, but with 30 configurations with the largest CI coefficients. The result is very similar to the CH_4 DCH Auger spectra in Fig. 2 which were calculated with 5 configurations with the largest CI coefficients. The details of the figure is the same as in the Fig. 2.

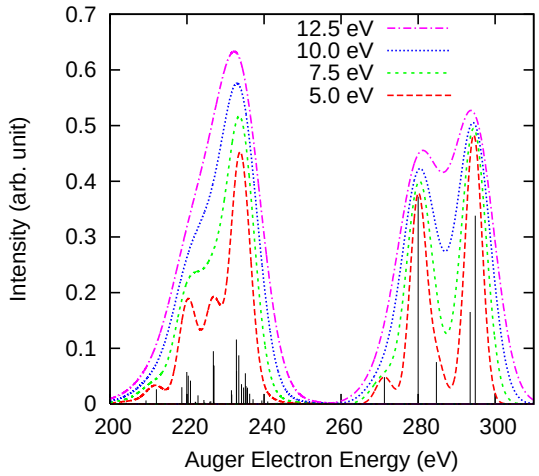

FIG. S2. Effect of Gaussian width used for convolution. The convoluted CH_4 DCH Auger spectra with different FWHM width are shown. Our result suggests that FWHM has strong influence on the shape of the Auger spectra, which may be important when we compare calculated spectrum with experimental result. The details of the figure is the same as in Fig. 2.

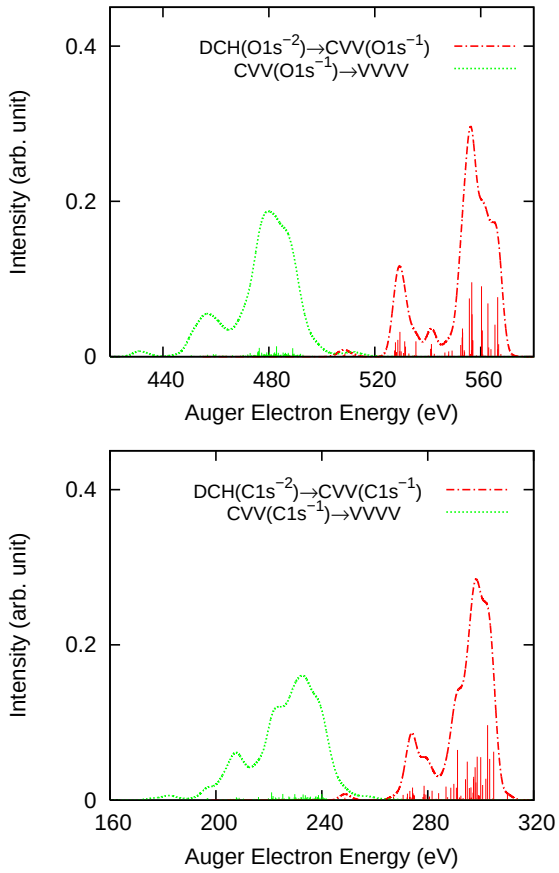

FIG. S3. H_2CO DCH → CVV and CVV → VVVV Auger spectra expected in SR experiment. In Fig. 8, we show H_2CO DCH Auger spectra expected for XFEL experiment. In case of SR experiment, formation efficiencies of the ts-DCH states are expected to be low, 1/100 of the ss-DCH states. Thus, we can ignore the ts-DCH contributions in simulating Auger spectra in SR experiment. In this figure, the Auger spectra without the ts-DCH contribution is shown. The details of the figure is the same as in Fig. 8.

TABLE I. Expressions of Auger decay amplitude t for transitions from ss-DCH, singlet ts-DCH and triplet ts-DCH states to CVV state, with assumptions of single configurational wave functions and frozen orbitals. "CVV S=1/2 (S)" represents doublet CVV state with singlet intermediate spin coupling of valence electrons, and "CVV S=1/2 (T)" represents doublet CVV state with triplet intermediate spin coupling of valence electrons. v and w refer to orbitals involved in the valence hole creation, c stands for inner-shell orbital involved in the core-hole decay, and k represents continuum orbital of Auger electron.

	ss-DCH	ts-DCH (singlet)	ts-DCH (triplet)
CVV S=1/2 (S)	$(kv\|cw)+(kw\|cv) \quad (v \neq w)$ $\sqrt{2}\,(kv\|cw) \quad (v = w)$	$\sqrt{\frac{1}{2}}\,[(kv\|cw)+(kw\|cv)] \quad (v \neq w)$ $(kv\|cw) \quad (v = w)$	$\sqrt{\frac{1}{2}}\,[(kv\|cw)+(kw\|cv)] \quad (v \neq w)$ $(kv\|cw) \quad (v = w)$
CVV S=1/2 (T)	$\sqrt{3}\,[(kv\|cw)-(kw\|cv)]$	$\sqrt{\frac{3}{2}}\,[(kv\|cw)-(kw\|cv)]$	$\sqrt{\frac{1}{6}}\,[(kv\|cw)-(kw\|cv)]$
CVV S=3/2	–	–	$\sqrt{\frac{4}{3}}\,[(kv\|cw)-(kw\|cv)]$

TABLE II. Representative CVV states of CH_4 molecule. Energy refers to the ionization energy with respect to the neutral ground state of CH_4. Intermediate spin means spin coupling in valence electrons, where S and T represent singlet and triplet, respectively.

State	Energy (eV)	Main configuration (Intermediate spin)	Intensity (arb.)
$^4T_1$	352.662	$(1s)^1(1t_2)^4$ (T)	-
^2E	354.362	$(1s)^1(1t_2)^4$ (S)	0.000
$^2T_1$	354.809	$(1s)^1(1t_2)^4$ (T)	0.000
$^2T_2$	355.358	$(1s)^1(1t_2)^4$ (S)	0.338
$^2A_1$	356.676	$(1s)^1(1t_2)^4$ (S)	0.165
$^4T_2$	361.996	$(1s)^1(2a_1)^1(1t_2)^5$ (T)	-
$^2T_2$	365.469	$(1s)^1(2a_1)^1(1t_2)^5$ (T)	0.075
$^2T_2$	370.181	$(1s)^1(2a_1)^1(1t_2)^5$ (S)	0.372
$^2A_1$	378.961	$(1s)^1(2a_1)^0$ (S)	0.048

TABLE III. Representative CVV states of NH_3 molecule. The other details are the same as in Table II.

State	Energy (eV)	Main configuration (Intermediate spin)	Intensity (arb.)
^4E	470.431	$(1s)^1(1e)^3(3a_1)^1$ (T)	-
$^2A_1$	470.810	$(1s)^1(3a_1)^0$ (S)	0.078
^2E	474.026	$(1s)^1(1e)^3(3a_1)^1$ (S)	0.168
^2E	475.207	$(1s)^1(1e)^3(3a_1)^1$ (T)	0.154
$^4A_2$	476.080	$(1s)^1(1e)^2$ (T)	-
$^2A_2$	479.240	$(1s)^1(1e)^2$ (T)	0.000
^2E	479.320	$(1s)^1(1e)^2$ (S)	0.134
$^2A_1$	480.593	$(1s)^1(1e)^2$ (S)	0.140
$^4A_1$	482.519	$(1s)^1(2a_1)^1(3a_1)^1$ (T)	-
^4E	487.973	$(1s)^1(2a_1)^1(1e)^1$ (T)	-
$^2A_1$	488.317	$(1s)^1(2a_1)^1(3a_1)^1$ (T)	0.049
$^2A_1$	491.578	$(1s)^1(2a_1)^1(3a_1)^1$ (S)	0.066
^2E	492.381	$(1s)^1(2a_1)^1(1e)^1$ (T)	0.056
^2E	497.398	$(1s)^1(2a_1)^1(1e)^1$ (S)	0.128
$^2A_1$	508.638	$(1s)^1(2a_1)^0$ (S)	0.020

TABLE IV. Low-lying C1s^{-1} CVV states of H_2CO molecule. C1s^{-2}, C1s^{-1}O1s^{-1} (S) and C1s^{-1}O1s^{-1} (T) are the initial states of the 1st Auger transitions, and represent the C1s^{-2} ss-DCH state, the singlet and triplet C1s^{-1}O1s^{-1} ts-DCH states, respectively. The other details are the same as in Table II.

			Intensity (arb.)		
State	Energy (eV)	Main configuration (Intermediate spin)	C1s^{-2}	C1s^{-1}O1s^{-1} (S)	C1s^{-1}O1s^{-1} (T)
$^2A_1$	347.931	$(2a_1)^1(2b_2)^0$ (S)	0.007	0.029	0.083
$^4A_2$	351.299	$(2a_1)^1(1b_1)^1(2b_2)^1$ (T)	-	-	0.000
$^2A_2$	351.646	$(2a_1)^1(1b_1)^1(2b_2)^1$ (T)	0.000	0.002	0.010
$^4A_1$	352.141	$(2a_1)^1(1b_2)^1(2b_2)^1$ (T)	-	-	0.024
$^4B_2$	352.408	$(2a_1)^1(2b_2)^1(5a_1)^1$ (T)	-	-	0.001
$^2B_2$	352.537	$(2a_1)^1(2b_2)^1(5a_1)^1$ (T)	0.000	0.001	0.000
$^2A_1$	353.532	$(2a_1)^1(1b_2)^1(2b_2)^1$ (T)	0.002	0.042	0.009
$^2A_2$	353.091	$(2a_1)^1(1b_1)^1(2b_2)^1$ (S)	0.063	0.068	0.200
$^2B_2$	354.603	$(2a_1)^1(2b_2)^1(5a_1)^1$ (S)	0.053	0.084	0.198
$^2A_1$	355.407	$(2a_1)^1(1b_2)^1(2b_2)^1$ (S)	0.097	0.005	0.063

TABLE V. Low-lying O1s^{-1} CVV states of H_2CO molecule. The other details are the same as in Table IV.

			Intensity (arb.)		
State	Energy (eV)	Main configuration (Intermediate spin)	O1s^{-2}	C1s^{-1}O1s^{-1} (S)	C1s^{-1}O1s^{-1} (T)
$^2A_1$	595.785	$(1a_1)^1(2b_2)^0$ (S)	0.001	0.040	0.080
$^4A_2$	598.722	$(1a_1)^1(1b_1)^1(2b_2)^1$ (T)	-	-	0.049
$^4A_1$	599.230	$(1a_1)^1(1b_2)^1(2b_2)^1$ (T)	-	-	0.037
$^2A_2$	599.395	$(1a_1)^1(1b_1)^1(2b_2)^1$ (S)	0.000	0.030	0.024
$^4B_2$	599.876	$(1a_1)^1(2b_2)^1(5a_1)^1$ (T)	-	-	0.006
$^2B_2$	600.951	$(1a_1)^1(2b_2)^1(5a_1)^1$ (T)	0.004	0.001	0.009
$^2A_1$	601.788	$(1a_1)^1(1b_2)^1(2b_2)^1$ (T)	0.016	0.013	0.001
$^2B_2$	602.113	$(1a_1)^1(2b_2)^1(5a_1)^1$ (S)	0.010	0.004	0.037
$^2A_2$	602.145	$(1a_1)^1(1b_1)^1(2b_2)^1$ (T)	0.077	0.001	0.034
$^4B_2$	602.876	$(1a_1)^1(2b_2)^1(4a_1)^1$ (T)	-	-	0.025
$^2A_1$	603.166	$(1a_1)^1(1b_2)^1(2b_2)^1$ (S)	0.041	0.007	0.061